

**Dr Charles JR Williams, BA DPhil FRGS
Research Fellow**

1.2n, School of Geographical Sciences
University Road, Bristol, BS8 1SS

Wednesday 10 June 2020

Dear Dr Loutre,

Re: Submission of manuscript “CMIP6/PMIP4 simulations of the mid-Holocene and Last Interglacial using HadGEM3: comparison to the pre-industrial era, previous model versions, and proxy data” by CJR Williams *et al.* to Climate of the Past (PMIP4 Special Edition).

Thank you very much for your most recent comments. I have now made all the corrections that you requested, so please see below for my responses:

1. Minor comment

I invite you to double check the writing of the supplementary material and make it 'easier' to read. In particular the first sentence (121-22) looks very strange to me. I think it would be worth to remind the readers what are GA, GC, GO, GIS (only the 'full words' for the acronyms, such as 'Global Atmosphere', 'Global Ocean', ... nothing more. And would it be possible to explain in a few words what you mean with 'bottom-up and top-down developments' (124-35)?

This has now been corrected, with the first sentence being changed so that it makes more logical sense (and is more independent from the main manuscript), the acronyms being listed, and that last sentence being removed (as we considered it ambiguous)

2. Major comment

Your data availability section does not comply with the requirements from COPERNICUS. I asked the Climate-of-Past co-editors-in-chief and I copy here the answer...

As requested, I have now added in the website to the ESGF portal, and have made it clearer that although my simulations have not yet been uploaded to this, they are nevertheless publicly available, by contacting myself. As I say in my manuscript, we plan to upload our simulations to the ESGF portal, and will do so in the near future. However, CMIP6 protocol states that the data must all be in a correct and consistent format - a process called CMORising - and this is a lengthy and nontrivial process. It would seriously delay publication of this manuscript if the data have to be uploaded to the ESGF before publication. I hope the clarification that I have added will satisfy your regulations? If not, would an acceptable alternative be that I provide climatologies of the relevant fields (temperature, precipitation etc) from the model simulations as a supplementary netcdf file? Please let me know the best option.

Lastly, I have also corrected the reference list, as per your comment in the email dated 2 June 2020:

Please note that your reference list has not been compiled according to our standards. Please consider adjusting your reference list with the next revision of your manuscript. The manuscript preparation guidelines can be seen at: https://www.climate-of-the-past.net/for_authors/manuscript_preparation.html.

This has now been corrected.

I very much hope that my manuscript now meets your technical specifications, and is deemed acceptable and ready for publication.

Yours sincerely,

A handwritten signature in cursive script, appearing to read "C. R. Williams". The signature is written in dark ink and is positioned above the typed name.

Dr Charles JR Williams, and co-authors

1 **CMIP6/PMIP4 simulations of the mid-Holocene and Last Interglacial using**
2 **HadGEM3: comparison to the pre-industrial era, previous model versions,**
3 **and proxy data**

4 **~~The UK contribution to CMIP6/PMIP4: mid-Holocene and Last~~**
5 **~~Interglacial experiments with HadGEM3, and comparison to the pre-~~**
6 **~~industrial era and proxy data~~**

7
8 **Charles J. R. Williams^{1,5}, Maria-Vittoria Guarino², Emilie Capron³, Irene Malmierca-**
9 **Vallet^{1,2}, Joy S. Singarayer^{4,1}, Louise C. Sime², Daniel J. Lunt¹, Paul J. Valdes¹**

10
11 ¹School of Geographical Sciences, University of Bristol, UK (c.j.r.williams@bristol.ac.uk)

12 ²British Antarctic Survey, Cambridge, UK

13 ³Physics of Ice, Climate and Earth, Niels Bohr Institute, University of Copenhagen, Denmark

14 ⁴Department of Meteorology & School of Archaeology, Geography and Environmental
15 Science, University of Reading, UK

16 ⁵NCAS-Climate / Department of Meteorology, University of Reading, UK

17
18
19
20
21
22
23
24
25
26 **Corresponding author address:**

27 Room 1.2n, School of Geographical Sciences,
28 University Road, Bristol, BS8 1SS
29 United Kingdom

30
31 Email: c.j.r.williams@bristol.ac.uk

32
33 Short title: mid-Holocene and Last Interglacial experiments with HadGEM3

34 Keywords: Palaeoclimate, Quaternary change, mid-Holocene, Last Interglacial

35 **ABSTRACT**

36 Palaeoclimate model simulations are an important tool to improve our understanding of the
37 mechanisms of climate change. These simulations also provide tests of the ability of models to
38 simulate climates very different to today. Here we present the results from two [brand-new](#)
39 simulations using the latest version of the UK's physical climate model, HadGEM3-GC3.1; the mid-
40 Holocene (~6 ka) and Last Interglacial (~127 ka) simulations, both conducted under the auspices of
41 CMIP6/PMIP4. [This is the first time this version of the UK model has been used to conduct](#)
42 [paleoclimate simulations.](#) These periods are of particular interest to PMIP4 because they represent the
43 two most recent warm periods in Earth history, where atmospheric concentration of greenhouse gases
44 and continental configuration ~~is~~ [are](#) similar to the pre-industrial period, but where there were
45 significant changes to the Earth's orbital configuration, resulting in a very different seasonal cycle of
46 radiative forcing.

47

48 Results for these simulations are assessed [firstly](#) against [the same model's preindustrial control](#)
49 [simulation \(a simulation comparison, to describe and understand the differences between the](#)
50 [preindustrial and the two paleoclimate simulations\), and secondly against previous versions of the](#)
51 [same model relative to newly-available proxy data \(a model-data comparison, to compare all available](#)
52 [simulations from the same model with proxy data to assess any improvements due to model](#)
53 [advances\), previous versions of the UK model, and models from the previous CMIP5 exercise. The](#)
54 [introduction of this newly available proxy data adds further novelty to this study. Globally, for](#)
55 [metrics such as 1.5m temperature and surface rainfall, whilst both the recent paleoclimate simulations](#)
56 [are mostly capturing the expected sign and, in some places, magnitude of change relative to the](#)
57 [preindustrial, this is geographically and seasonally dependent. Compared to newly-available proxy](#)
58 [data \(including SST and rainfall\), and also incorporating data from previous versions of the model,](#)
59 [shows that the relative accuracy of the simulations appears to vary according to metric, proxy](#)
60 [reconstruction used for comparison and geographical location. In some instances, such as mean](#)
61 [rainfall in the mid-Holocene, there is a clear and linear improvement, relative to proxy data, from the](#)
62 [oldest to the newest generation of the model. When zooming into northern Africa, a region known to](#)
63 [be problematic for models in terms of rainfall enhancement, the behaviour of the West African](#)
64 [monsoon in both recent paleoclimate simulations is consistent with current understanding, suggesting](#)
65 [a wetter monsoon during the mid-Holocene and \(more so\) the Last Interglacial, relative to the](#)
66 [preindustrial era. However, regarding the well-documented 'Saharan greening' during the mid-](#)
67 [Holocene, results here suggest that the most recent version of the UK's physical model is still unable](#)
68 [to reproduce the increases suggested by proxy data, consistent with all other previous models to date.](#)
69 ~~When the current version is compared to the previous generation of the UK model, the most recent~~
70 ~~version suggests limited improvement. In common with these previous model versions, the~~
71 ~~simulations reproduce global land and ocean temperatures (both surface and at 1.5 m) and a West~~

72 African monsoon that is consistent with the latitudinal and seasonal distribution of insolation. The
73 Last Interglacial simulation appears to accurately capture Northern Hemisphere temperature changes,
74 but without the addition of Last Interglacial meltwater forcing cannot capture the magnitude of
75 Southern Hemisphere changes. Model-data comparisons indicate that some geographical regions, and
76 some seasons, produce better matches to the palaeodata (relative to pre-industrial) than others.
77 Model-model comparisons, relative to previous generations same model and other models, indicate
78 similarity between generations in terms of both the intensity and northward enhancement of the mid-
79 Holocene West African monsoon, both of which are underestimated. On the ‘Saharan greening’
80 which occurred the mid-Holocene African Humid Period, simulation results are likewise consistent
81 with other models. The most recent version of the UK model appears to still be unable to reproduce
82 the amount of rainfall necessary to support grassland across the Sahara.

83

84 1. INTRODUCTION

85 Simulating past climates has been instrumental in improving our understanding of the mechanisms of
86 climate change (e.g. Gates 1976, Haywood *et al.* 2016, Jungclaus *et al.* 2017, Kageyama *et al.* 2017,
87 Kageyama *et al.* 2018, Kohfeld *et al.* 2013, Lunt *et al.* 2008, Otto-Bliesner *et al.* 2017, Ramstein *et al.*
88 1997), as well as in identifying and assessing discrepancies in palaeoclimate reconstructions (e.g.
89 Rind & Peteet 1985). Palaeoclimate scenarios can also provide tests of the ability of models to
90 simulate climates that are very different to today, often termed ‘out-of-sample’ tests. This notion
91 underpins the idea that robust simulations of past climates improve our confidence in future climate
92 change projections (Braconnot *et al.* 2011, Harrison *et al.* 2014, Taylor *et al.* 2011). Palaeoclimate
93 scenarios have also been used to provide additional tuning targets for models (e.g. Gregoire *et al.*
94 2011), in combination with historical or pre-industrial conditions.

95

96 The international Climate Model Intercomparison Project (CMIP) and the Palaeoclimate Model
97 Intercomparison Project (PMIP) have spearheaded the coordination of the international palaeoclimate
98 modelling community to run key scenarios with multiple models, perform data syntheses, and
99 undertake model-data comparisons since their initiation twenty-five years ago (Joussaume & Taylor
100 1995). Now in its fourth incarnation, PMIP4 (part of the sixth phase of CMIP, CMIP6), it includes a
101 larger set of models than previously, and more palaeoclimate scenarios and experiments covering the
102 Quaternary (documented in Jungclaus *et al.* 2017, Kageyama *et al.* 2017, Kageyama *et al.* 2018 and
103 Otto-Bliesner *et al.* 2017) and Pliocene (documented in Haywood *et al.* 2016).

104

105 PMIP4 specifies experiment set-ups for two ~~warm~~ interglacial simulations: the mid-Holocene (MH) at
106 ~6 ka and the Last Interglacial (LIG) at ~127 ka (although spanning covering ~129-116 ka in its
107 entirety). These are the two most recent warm periods (particularly in the Northern Hemisphere) in
108 Earth history, and are of particular interest to PMIP4; indeed, the MH experiment is one of the two
109 entry cards into PMIP (Otto-Bliesner *et al.* 2017). This is because whilst the atmospheric
110 concentration of greenhouse gases, the extent of land ice, and the continental configuration is similar
111 in these PMIP4 set-ups compared to the pre-industrial (PI) period, significant changes to the seasonal
112 cycle of radiative forcing, relative to today, do occur during these periods due to long-term variations
113 in the Earth’s orbital configuration. The MH and LIG both have higher boreal summer insolation and
114 lower boreal winter insolation compared to the PI, as shown by Figure 1, leading to an enhanced
115 seasonal cycle in insolation as well as a change in its latitudinal distribution. The change is more
116 significant in the LIG than the MH, due to the larger eccentricity of the Earth’s orbit at that time.
117 Note that, in this figure and indeed all subsequent figures using monthly or seasonal data, the data
118 have been calendar adjusted (Joussaume & Braconnot 1997) according to the method of Pollard &
119 Reusch (2002) and Marzocchi *et al.* (2015); see the Supplementary Material (SM1) for the same
120 figure but using the modern calendar.

121

122 Palaeodata syntheses indicate globally warmer surface conditions of potentially $\sim 0.7^{\circ}\text{C}$ than PI in the
123 MH (Marcott *et al.* 2013) and up to $\sim 1.3^{\circ}\text{C}$ in the LIG (Fischer *et al.* 2018). During both warm
124 periods there is abundant palaeodata evidence indicating enhancement of Northern Hemisphere
125 summer monsoons (e.g. Wang *et al.* 2008) and in the case of the Sahara, replacement of desert by
126 shrubs and steppe vegetation (e.g. Drake *et al.* 2011, Hoelzmann *et al.* 1998), grassland and
127 xerophytic woodland/scrubland (e.g. Jolly *et al.* 1998a, Jolly *et al.* 1998b, Joussaume *et al.* 1999) and
128 inland water bodies (e.g. Drake *et al.* 2011, Lezine *et al.* 2011). -Recent palaeodata compilations
129 involving either air temperatures or SST (Capron *et al.* 2014, Hoffman *et al.* 2017) reveal that the
130 maximum temperatures were reached asynchronously in the LIG between the Northern and Southern
131 Hemispheres. Concerning precipitation, historically this has been lacking relative to temperature or
132 SST reconstructions. One often-cited study for the MH is that of Bartlein *et al.* (2011), comprising a
133 combination of existing quantitative reconstructions based on pollen and plant macrofossils; this
134 provides evidence of the interaction between orbital variations and greenhouse gas forcing, and the
135 atmospheric circulation response. More recently, one newly-published dataset of LIG precipitation
136 proxy data (which the current study benefits from as part of the model-data comparison, see below) is
137 that of Scussolini *et al.* (2019). Here, a number of climate models are assessed against this brand-new
138 dataset, finding an agreement with proxy data over Northern Hemisphere landmasses, but less so in
139 the Southern Hemisphere (Scussolini *et al.* 2019).

140

141 Many modelling studies have been undertaken in an attempt to reproduce the changes suggested by
142 proxy data throughout the Quaternary, and especially during the interglacial periods discussed here,
143 and there is not scope in this current study to give a full review here. An overview of multi-model
144 assessments during the LIG can be found in Lunt *et al.* (2013). However, one example is the
145 aforementioned monsoon enhancement (and expansion/contraction) during the Quaternary, and
146 previous studies have focused on various aspects of this, such as whether any expansion was
147 hemispherically consistent or asynchronous between hemispheres (e.g. Kutzbach *et al.* 2008, McGee
148 *et al.* 2014, Singarayer & Burrough 2015, Singarayer *et al.* 2017, Wang *et al.* 2006, Wang *et al.*
149 2014). During the LIG, the aforementioned asynchronous temperature distribution between the
150 hemispheres ~~Furthermore, has been investigated by a number of model simulations, suggest~~
151 suggesting that this may have been caused by meltwater induced shutdown of the Atlantic Meridional
152 Overturning Circulation (AMOC) in the early part of the LIG, due to the melting of the Northern
153 Hemisphere ice sheets during the preceding deglaciation (e.g. Carlson 2008, Smith & Gregory 2009,
154 Stone *et al.* 2016). ~~During both warm periods there is abundant palaeodata evidence indicating~~
155 ~~enhancement of Northern Hemisphere summer monsoons (e.g. Wang *et al.* 2008) and in the case of~~

156 ~~the Sahara, replacement of desert by shrubs and steppe vegetation (e.g. Drake *et al.* 2011, Hoelzmann~~
157 ~~*et al.* 1998) and inland water bodies (e.g. Drake *et al.* 2011, Lezine *et al.* 2011).~~

158
159 The driving mechanism producing the climate and environmental changes indicated by the palaeodata
160 for the ~~MH and LIG~~ ~~and MH~~ is different to current and future anthropogenic warming, as the former
161 results from orbital forcing changes whilst the latter results from increases in greenhouse gases.
162 Moreover, the orbital forcing primarily acts on shortwave radiation whereas greenhouse gas changes
163 primarily act upon the longwave radiation flux, and the orbital forcing can lead to uneven horizontal
164 and seasonal changes whereas greenhouse gas forcing can cause more uniform anomalies (it should
165 be noted that whilst a precise calculation of the radiative forcing due to changes in MH and LIG
166 greenhouse gases is beyond the scope of this study, such a calculation could follow the methodology
167 of Gunnar *et al.* [1998]). Nevertheless, despite these differences in driving mechanism, However,
168 these past high latitude (and mainly Northern Hemisphere) warm intervals are a unique opportunity to
169 understand the magnitudes of forcings and feedbacks in the climate system that produce warm
170 interglacial conditions, which can help us understand and constrain future climate projections (e.g.
171 Holloway *et al.* 2016, Rachmayani *et al.* 2017, Schmidt *et al.* 2014). Running the same model
172 scenarios with ever newer models enables the testing of whether model developments are producing
173 improvements in palaeo model-data comparisons, assuming appropriate boundary conditions are used.
174 Previous iterations of PMIP, with older versions of the PMIP4 models, have uncovered persistent
175 shortcomings (Harrison *et al.* 2015) that have not been eliminated despite developments in resolution,
176 model physics, and addition of further Earth system components. One key example of this is the
177 continued underestimation of the increase in rainfall over the Sahara in the MH PMIP simulations
178 (e.g. Braconnot *et al.* 2012).

179
180 In this study we run and assess the latest version of the UK's physical climate model, HadGEM3-
181 GC3.1. Whilst older versions of the UK model have been included in previous iterations of CMIP,
182 and whilst present-day and future simulations from this model are included in CMIP6, the novelty of
183 this study is that this is the first time this version has been used to conduct any paleoclimate
184 simulations. In Global Coupled (GC) version 3 (and therefore in the following GC3.1), there have
185 been many updates and improvements, relative to its predecessors, which are discussed extensively in
186 Williams *et al.* (2017) and a number of companion scientific model development papers (see Section
187 2.1). As a brief introduction, however, GC3 includes a new aerosol scheme, multilayer snow scheme,
188 multilayer sea ice and several other parametrization changes, including a set relating to cloud and
189 radiation, as well as a revision to the numerics of atmospheric convection (Williams *et al.* 2017). In
190 addition, the ocean component of GC3 has other changes including ~~a new~~ an updated ocean and sea
191 ice model, a new cloud scheme, and further revisions to all parametrization schemes (Williams *et al.*
192 2017). See Section 2.1 for further details.

193

194 Following the CMIP6/PMIP4 protocol, here the PMIP4 MH and LIG simulations have been
195 conducted and assessed, with the assessment adopting a two-pronged approach. -Firstly a simulation
196 comparison is made between these simulations and the same model's PI simulation (to describe and
197 understand the differences between them). Secondly a model-data comparison is made between the
198 current and previous versions of the same model relative to newly-available proxy data, thereby
199 assessing any improvements due to model advances~~comparing the results with available proxy data,~~
200 ~~previous versions of the UK's same physical climate model, and other models from CMIP5. In~~
201 addition to a global assessment, a secondary ~~The~~ focus of this paper is on the fidelity of the
202 temperature anomalies ~~globally~~ and the degree of precipitation enhancement in the Sahara, the latter
203 of which has proved problematic for several generations of models. ~~The results discussed here are~~
204 ~~split into two sections: after an assessment of the level of equilibrium gained during the spin-up phase,~~
205 ~~the main focus is on the model data and model-model comparisons using the production runs.~~
206 Following this introduction, Section 2 describes the model, the experimental design, ~~and~~ the proxy
207 data used for the model-data comparisons, and a brief discussion of the simulation spin-up phases.
208 Section 3 then presents the results, beginning with the model-model comparison and following with
209 the model-data comparison, and -fdivided into two subsections: i) equilibrium during the spin-up
210 phase; and ii) model data and model-model comparisons from the production runs. Finally/finally,
211 section 4 summarises and concludes.

212

213 **2. MODEL, EXPERIMENT DESIGN, ~~AND DATA~~ AND SPIN-UP SIMULATIONS**

214 **2.1. Model**

215 **2.1.1. Model terminology**

216 In this paper, and consistent with CMIP nomenclature, the 'spin-up phase' of the simulations refers to
217 when they are spinning up to atmospheric and oceanic equilibrium, whereas the 'production run'
218 refers to the end parts (usually the last 50 or 100 years) of the simulation used to calculate the
219 climatologies, presented as the results. When discussed as geological intervals, the preindustrial, mid-
220 Holocene and Last Interglacial are referred to as the PI, MH and LIG respectively. In contrast, when
221 discussed as the three most recent simulations using HadGEM3 (see below), consistent with CMIP
222 they are referred to as the *piControl*, *midHolocene* and *lig127k* simulations, respectively. When the
223 *midHolocene* and *lig127k* are discussed collectively, they are referred to as the 'warm climate
224 simulations'; whilst it is acknowledged that other factors differentiate these simulations such as orbital
225 configuration or CO₂, 'warm climate simulations' was deemed an appropriate collective noun.

226

227 **2.1.2. Model details**

228 ~~The MH and LIG simulations conducted here (referred to as *midHolocene* and *lig127k*, respectively,~~
229 ~~and collectively as the warm climate simulations~~ conducted here), and ~~indeed~~ the *piControl* PI

230 simulation (~~piControl~~, conducted elsewhere as part of the UK's CMIP6 runs and used here for
231 comparative purposes) were all run using the same fully-coupled GCM: the Global Coupled 3
232 configuration of the UK's physical climate model, HadGEM3-GC3.1. Full details on HadGEM3-
233 GC3.1, and a comparison to previous configurations, are given in Williams *et al.* (2017) and
234 Kuhlbrodt *et al.* (2018). Here, the model was run using the Unified Model (UM), version 10.7, and
235 including the following components: i) Global Atmosphere (GA) version 7.1, with an N96
236 atmospheric spatial resolution (approximately 1.875° longitude by 1.25° latitude) and 85 vertical
237 levels; ii) the NEMO ocean component, version 3.6, including Global Ocean (GO) version 6.0
238 (ORCA1), with an isotropic Mercator grid which, despite varying in both meridional and zonal
239 directions, has an approximate spatial resolution of 1° by 1° and 75 vertical levels; iii) the Global Sea
240 Ice (GIS) component, version 8.0 (GSI8.0); iv) the Global Land (GL) configuration, version 7.0, of
241 the Joint UK Land Environment Simulator (JULES); and v) the OASIS3 MCT coupler. The official
242 title for this configuration of HadGEM3-GC3.1 is HadGEM3-GC31-LL N96ORCA1 UM10.7
243 NEMO3.6 (for brevity, hereafter HadGEM3).

244
245 All of the above individual components are summarised by Williams *et al.* (2017) and detailed
246 individually by a suite of companion papers (see Walters *et al.* 2017 for GA7 and GL7, Storkey *et al.*
247 2017 for GO6 and Ridley *et al.* 2017 for GIS8). However, a brief description of the major changes
248 relative to its predecessor are given [in the Supplementary Material here](#). ~~Beginning with GA7 and~~
249 ~~GL7, a once in a decade replacement of the model's dynamical core, implementing ENDGame, was~~
250 ~~undertaken for the previous version (GA6) and therefore remains the same in GA7 (Walters *et al.*~~
251 ~~2017). In addition, a number of bottom up and top down developments were included in GA7. For~~
252 ~~the former, these include improvements to the radiation scheme to allow better treatment of gases~~
253 ~~absorption, improvements to how warm rain and ice clouds are treated, and an improvement to the~~
254 ~~numerics of the convection scheme (Walters *et al.* 2017). For the latter, these include further~~
255 ~~improvements to the microphysics as well as an incremental development of ENDGame (Walters *et*~~
256 ~~*al.* 2017). Together these led to reductions in four model errors that were deemed critical in the~~
257 ~~previous configuration: i) South Asian monsoon rainfall biases over India; ii) biases in both~~
258 ~~temperature and humidity in the tropical tropopause; iii) shortcomings in the numerical conservation;~~
259 ~~and iv) biases in surface radiation fluxes over the Southern Ocean (Walters *et al.* 2017). In addition to~~
260 ~~these developments, two new parameterisation schemes were introduced in GA7: firstly the UK~~
261 ~~Chemistry and Aerosol (UKCA) GLOMAP mode aerosol scheme, to improve the representation of~~
262 ~~tropospheric aerosols, and secondly a multi-layer snow scheme in JULES, to allow the first time~~
263 ~~inclusion of stochastic physics in UM climate simulations (Walters *et al.* 2017).~~

264
265 ~~For the GO and GIS components, a number of improvements to GO6 have been made since the~~
266 ~~previous version, the first of which was an upgrade of the NEMO base code (to version 3.6) which~~

267 allowed a formulation for momentum advection (from Hollingsworth *et al.* 1983), a Lagrangian
268 icebergs scheme, and a simulation of circulation below ice shelves (Storkey *et al.* 2018). Other
269 developments included an improvement to the warm SST bias in the Southern Ocean (as detailed by
270 Williams *et al.* 2017), as well as tuning to various parameters e.g. the isopycnal diffusion (Storkey *et*
271 *al.* 2018). For GIS8, along with improvements to the albedo scheme and more realistic semi-implicit
272 coupling, the biggest development since its predecessor is the inclusion of multilayer
273 thermodynamics, giving a heat capacity to the sea ice and allowing vertical variation of conduction
274 (Ridley *et al.* 2018). Testing of these two components produced a better simulation compared to its
275 predecessor, with more realistic mixed layer depths in the Southern Ocean and the aforementioned
276 reduced warm bias, the latter of which was deemed primarily due to the tuning of the different mixing
277 (e.g. vertical and isopycnal) parameters (Storkey *et al.* 2018).

278
279 When all of these components are coupled together to give GC3, there have been several
280 improvements relative to its predecessor (GC2), most noticeably to the large warm bias in the
281 Southern Ocean (which was reduced by 75%), as well as an improved simulation of clouds, sea ice,
282 the frequency of tropical cyclones in the Northern Hemisphere as well as the AMOC, and the Madden
283 Julian Oscillation (MJO) (Williams *et al.* 2017). Relative to the previous fully-coupled version of the
284 model (HadGEM2), which was submitted to the last CMIP5/PMIP3 exercise, many systematic errors
285 have been improved ~~including a reduction of the temperature bias in many regions~~
286 ~~reduction in many regions to the temperature bias~~, a better simulation of mid-latitude synoptic
287 variability, and an improved simulation of tropical cyclones and the El Niño Southern Oscillation
288 (ENSO) (Williams *et al.* 2017).

289
290 Here, the *midHolocene* and *lig127k* simulations were both run on the UK National Supercomputing
291 Service, ARCHER, whereas the *piControl* was run on a different platform based within the UK Met
292 Office's Hadley Centre. While this may mean that anomalies computed against the *piControl* are
293 potentially influenced by different computing environments, and not purely the result of different
294 climate forcings, the reproducibility of GC3.1 simulations across different platforms has been tested
295 (Guarino *et al.* 2020). It was found that, although a simulation length of 200 years is recommended
296 whenever possible to adequately capture climate variability across different platforms, the main
297 climate variables considered here (e.g. surface temperature) are not expected to be significantly
298 different on a 100- or 50-year timescale (see, for example, Fig. 6 in Guarino *et al.* [2020]) as they
299 are not directly affected by medium-frequency climate processes ~~such as ENSO~~.

300
301 ~~Not including queueing time, both simulations were achieving 3-4 model years per day during the~~
302 ~~spin-up phase, and 1-2 model years per day during the production run; see below for the differences in~~
303 ~~output, and therefore speed, between the two phases.~~

304

305 2.2. Experiment design

306 Full details of the experimental design, and results from the CMIP6 *piControl* simulation, are
307 documented in Menary *et al.* (2018). Both the warm climate simulations followed the experimental
308 design given by Otto-Bliesner *et al.* (2017), and specified at
309 https://pmip4.lsce.ipsl.fr/doku.php/exp_design:index. The primary differences from the *piControl*
310 were to the astronomical parameters and the atmospheric trace greenhouse gas concentrations,
311 summarised in Table 1. For the astronomical parameters, these were prescribed in Otto-Bliesner *et al.*
312 (2017) according to orbital constants from Berger & Loutre (1991). However, in HadGEM3, the
313 individual parameters (e.g. eccentricity, obliquity, etc) use orbital constants based on Berger (1978),
314 according to the specified start date of the simulation. For the atmospheric trace greenhouse gas
315 concentrations, these were based on recent reconstructions from a number of sources (see Table 1 for
316 values, and section 2.2 in Otto-Bliesner *et al.* [2017] for a full list of references/sources).

317

318 All other boundary conditions, including solar activity, ice sheets, topography and coastlines, volcanic
319 activity and aerosol emissions, are identical to the CMIP6 *piControl* simulation. Likewise, vegetation
320 was prescribed to present-day values, to again match the CMIP6 *piControl* simulation. As such, the
321 *piControl* and both the warm climate simulations actually include a prescribed fraction of urban land
322 surface. As a result of this, our orbitally- and greenhouse gas-forced simulations should be considered
323 as anomalies to the *piControl*, rather than absolute representations of the MH or LIG climate.

324

325 Both the warm climate simulations were started from the end of the *piControl* spin-up phase (which
326 ran for approximately 600 years), after which time the *piControl* was considered to be in atmospheric
327 and oceanic equilibrium (Menary *et al.* 2018). To assess this, four metrics were used, namely net
328 radiative balance at the top of the atmosphere (TOA), surface air temperature (SAT), ~~and~~ full-depth
329 ocean temperature (OceTemp) and [full-depth ocean](#) salinity (OceSal) (Menary *et al.* (2018). See
330 [Section 3.1 2.4](#) (and in particular Table 2) for an analysis of the equilibrium state of both the
331 *piControl* and the warm climate simulations. Starting at the end of the *piControl*, these were then run
332 for their own spin-up phases, 400 and 350 years for the *midHolocene* and *lig127k* respectively.

333 ~~During this phase, ~700 diagnostics were output, containing mostly low temporal frequency (e.g.~~
334 ~~monthly, seasonal and annual) fields.~~ Once the simulations were considered in an acceptable level of
335 equilibrium (see [Section 3.1 2.4](#)), a production phase was run for 100 and 200 years for the
336 *midHolocene* and *lig127k* respectively, during which the full CMIP6/PMIP4 diagnostic profile
337 ~~(totalling ~1700 fields)~~ was implemented to output both high and low temporal frequency variables.

338

339 2.3. Data

340 Recent data syntheses compiling quantitative surface temperature and rainfall reconstructions were
341 used in order to evaluate the warm climate simulations.

342
343 For the MH, the global-scale continental surface mean annual temperature (MAT) and rainfall (or
344 mean annual precipitation, MAP) reconstructions from Bartlein *et al.* (2011), with quantitative
345 uncertainties accounting for climate parameter reconstruction methods, were used (see Data
346 Availability for access details). They rely on a combination of existing quantitative reconstructions
347 based on pollen and plant macrofossils and are inferred using a variety of methods (see Bartlein *et al.*
348 2011 for further details). At each site, the 6 ka anomaly (corresponding to the 5.5-6.5 ka average
349 value), is given relative to the present day, and in the case where modern values could not be directly
350 inferred from the record, modern climatology values (1961-1990) were extracted from the Climate
351 Research Unit historical climatology data set (New *et al.* 2002). [Further proxy data for the MH, such
352 as SST reconstructions, are not included here, as an extensive model-data comparison is presented in a
353 companion paper \(Brierley *et al.* 2020\).](#)

354
355 For the LIG, two [recent](#) different sets of surface temperature data are available. Firstly, the Capron *et al.*
356 (2017) 127 ka timeslice of SAT and sea surface temperature (SST) anomalies (relative to pre-
357 industrial, 1870-1899), is based on polar ice cores and marine sediment data that are (i) located
358 poleward of 40° latitude and (ii) have been placed on a common temporal framework (see Data
359 Availability for access details). Polar ice core water isotope data are interpreted as annual [mean](#)
360 surface air temperatures, while most marine sediment-based reconstructions are interpreted as summer
361 [\(defined here as July-September, JAS\)](#) SST signals. For each site, the 127 ka value was calculated as
362 the average value between 126 and 128 ka using the surface temperature curve resampled every 0.1
363 ka. [Here, we use the SST anomalies only.](#) Secondly, a global-scale time slice of SST anomalies,
364 relative to pre-industrial (1870-1889), at 127 ka was built, based on the recent compilation from
365 Hoffman *et al.* (2017), which includes both annual and summer SST reconstructions (see Data
366 Availability for access details). [This adds further novelty to this study, by using a new combined
367 dataset based on this existing data.](#) The 127 ka values at each site were extracted, following the
368 methodology they proposed for inferring their 129, 125 and 120 ka time slices i.e. the SST value at
369 127 ka was taken on the provided mean 0.1 ka interpolated SST curve for each core location. Data
370 syntheses from both Capron *et al.* (2014, 2017) and Hoffman *et al.* (2017) are associated with
371 quantitative uncertainties accounting for relative dating and surface temperature reconstruction
372 methods. Here, the two datasets are treated as independent data benchmarks, as they use different
373 reference chronologies and methodologies to infer temporal surface temperature changes, and
374 therefore they should not be combined. See Capron *et al.* (2017) for a detailed comparison of the two
375 syntheses. A model-data comparison exercise using existing LIG data compilations focusing on
376 continental surface temperature (e.g. Turney and Jones 2010) was not attempted, as they do no benefit

377 yet from a coherent chronological framework, preventing the definition of a robust time slice
378 representing the 127 ka terrestrial climate conditions (Capron *et al.* 2017).

379

380 [A brand-new, recently-published dataset of proxy precipitation anomalies \(again, relative to the](#)
381 [preindustrial\) is also used for model-data comparison purposes here, adding further novelty to this](#)
382 [study. The proxy data are compiled from existing literature by Scusscolini *et al.* \(2019\), and the](#)
383 [dataset includes 138 proxy locations from a number of paleoclimatic archives including pollen, fossils](#)
384 [other than pollen, lacustrine or marine sediment composition, loess deposits, and other multi-proxy](#)
385 [sources. Note that, as Scusscolini *et al.* \(2019\) observe, unlike temperature anomalies the majority of](#)
386 [precipitation anomalies in the existing literature are not quantitative. To allow a quantitative](#)
387 [comparison, Scusscolini *et al.* \(2019\) use a semi-quantitative scale, based on their expert judgement,](#)
388 [to show a LIG that is ‘much wetter’, ‘wetter’, ‘no discernible change’, ‘drier’ and ‘much drier’,](#)
389 [relative to the PI. The same scale is therefore used here. See Scusscolini *et al.* \(2019\) for further](#)
390 [information, and see Data Availability for access details\).](#)

391

392 **[2.4. Spin-up simulations](#)**

393 [As briefly mentioned above, both the warm climate simulations had a spin-up phase before the main](#)
394 [production run was started—, briefly discussed here. As an example of atmospheric equilibrium,](#)
395 [A annual global mean 1.5 m air temperature and TOA radiation from both warm climate simulations,](#)
396 [compared to the *piControl*, are shown in \[Fig. atmos. equilib\]\(#\) and summarised in Table 2; see](#)
397 [Supplementary Material \(SM2\) for the timeseries of these fields. There is a clear increase in](#)
398 [temperature during the beginning of this period, as the *piControl* slowly spins up from its original](#)
399 [starting point; this levels off towards the end of the period, however, with a final temperature trend of](#)
400 [0.03°C century⁻¹ \(Table 2 and \[Fig. atmos. equilib a\]\(#\)\).— For the warm climate simulations, despite](#)
401 [considerable interannual variability and arguably more so than in the *piControl* \(particularly halfway](#)
402 [through the *lig127k* simulation see SM2\), both are showing small long-term trends of -0.06°C century⁻¹](#)
403 [and -0.16°C century⁻¹ for the last 100 years of the *midHolocene* and *lig127k*, respectively \(Table 2](#)
404 [and \[Fig. atmos. equilib a\]\(#\)\).— The spatial patterns of these trends, also shown in the Supplementary](#)
405 [Material \(SM3\), are similar in both warm climate simulations, with much of the statistically](#)
406 [significant cooling occurring over high latitude regions in both Hemispheres, and particularly so over](#)
407 [Antarctica in the *lig127k* simulation \(SM3\). ~~The same is true for~~ The TOA radiation balance is also](#)
408 [showing long-term \(and again slightly negative\) trends by the end of the simulations, with -0.05 W m²](#)
409 [and -0.06 W m² for the the *midHolocene* and *lig127k*, respectively, where the *piControl* has a slow](#)
410 [downward trend towards zero until equilibrium was reached, whereas the *midHolocene* and *lig127k*](#)
411 [are relatively stable \(\[Fig. atmos. equilib b\]\(#\)\).](#)

412

413 For the oceanAs an example of oceanic equilibrium, annual global mean full-depth OcéTemp and
414 OcéSal are shown in Table 2 (and again visualised in the Supplementary Material, SM4) and
415 Fig_ocean_equilib. There is again a clear increase in OcéTemp during the *piControl* spin-up phase,
416 which again stabilises at 0.035°C century⁻¹ by the end of the period (Table 2). OcéTemp is steadily
417 increasing throughout the *piControl*, and this continues to increase in the *lig127k* until it stabilises
418 within the last ~50 years in both warm climate simulations(Fig_ocean_equilib a), whereas there is a
419 dramatic fall in ocean salinity in these simulations (SM4). A similar pattern is shown in OcéSal, with
420 a steady decrease in the *piControl* spin-up phase which continues during the *midHolocene* and,
421 conversely, starts to increase before stabilising during the *lig127k* (Fig_ocean_equilib b). Concerning
422 the long-term trends, Menary et al. (2018) considered values acceptable for equilibrium to be < +/-
423 0.035°C century⁻¹ and < +/-0.0001 psu century⁻¹ (for OcéTemp and OcéSal, respectively); as shown in
424 Table 2, although both warm climate simulations meet the temperature criterion, the *midHolocene*
425 neither meet the it is not meeting the salinity criterion (-0.00047 psu and 0.006 psu for the
426 *midHolocene* and *lig127k*, respectively, compared to a criterion of 0.0001 psu). However, running for
427 several thousands of years (and > 5 years of computer time), which would be needed to reach true
428 oceanic equilibrium, was simply unfeasible here given time and resource constraints.

429

430 3. RESULTS

431 ~~As briefly mentioned above, both the warm climate simulations had a spin-up phase before the main~~
432 ~~production run was started. The results discussed here are therefore split into two sections: firstly,~~
433 ~~assessing the level of atmospheric and oceanic equilibrium during (and, in particular, at the end of)~~
434 ~~the spin-up phase, and secondly assessing the 100-year climatology from the production run.~~

435

436 3.1. Spin-up

437 ~~Annual global mean 1.5 m air temperature and TOA radiation from both warm climate simulations,~~
438 ~~compared to the *piControl*, are shown in Fig_atmos_equilib and summarised in Table 2. Note that the~~
439 ~~*piControl* spin-up phase was run in three separate parts, to accommodate for minor changes/updates in~~
440 ~~the model as the simulation progressed. There is a clear increase in temperature during the beginning~~
441 ~~of this period, as the *piControl* slowly spins up from its original starting point; this levels off towards~~
442 ~~the end of the period, however, with a final temperature trend of 0.03°C century⁻¹ (Table 2 and~~
443 ~~Fig_atmos_equilib a). For the warm climate simulations, despite considerable interannual variability~~
444 ~~(particularly halfway through the *lig127k* simulation) both are showing small long-term trends of~~
445 ~~0.06°C century⁻¹ and 0.16°C century⁻¹ for the last 100 years of the *midHolocene* and *lig127k*,~~
446 ~~respectively (Table 2 and Fig_atmos_equilib a). The same is true for TOA, where the *piControl* has a~~
447 ~~slow downward trend towards zero until equilibrium was reached, whereas the *midHolocene* and~~
448 ~~*lig127k* are relatively stable (Fig_atmos_equilib b).~~

449

450 ~~For the ocean, annual global mean OecTemp and OecSal are shown in Table 2 and~~
451 ~~Fig_ocean_equilib. There is again a clear increase in OecTemp during the *piControl* spin-up phase,~~
452 ~~which again stabilises at $0.035^{\circ}\text{C century}^{-1}$ by the end of the period (Table 2). Whilst OecTemp~~
453 ~~stabilises in the *midHolocene* and indeed has a smaller trend than the *piControl* (Table 2), it continues~~
454 ~~to increase in the *lig127k* until it stabilises within the last 50 years (Fig_ocean_equilib a). A similar~~
455 ~~pattern is shown in OecSal, with a steady decrease in the *piControl* spin-up phase which continues~~
456 ~~during the *midHolocene* and, conversely, starts to increase before stabilising during the *lig127k*~~
457 ~~(Fig_ocean_equilib b). Concerning the long term trends, Menary *et al.* (2018) considered values~~
458 ~~acceptable for equilibrium to be $\leq \pm 0.035^{\circ}\text{C century}^{-1}$ and $\leq \pm 0.0001 \text{ psu century}^{-1}$ (for OecTemp~~
459 ~~and OecSal, respectively); as shown in Table 2, although both warm climate simulations meet the~~
460 ~~temperature criterion, neither meet the salinity criterion (-0.007 psu and 0.006 psu for the~~
461 ~~*midHolocene* and *lig127k*, respectively, compared to a criterion of 0.0001 psu). However, running for~~
462 ~~several thousands of years (and > 5 years of computer time), which would be needed to reach true~~
463 ~~oceanic equilibrium, was simply unfeasible here given time and resource constraints.~~

464

465 **3.21. Production runs results**

466 The warm climate production runs were undertaken following the spin-up phase, with ~~a 100-year~~ the
467 climatology of each simulation being compared to that from the *piControl*, as well as available proxy
468 data, using either annual means or summer/winter seasonal means. For the latter, depending on the
469 availability of the proxy data, Northern Hemisphere summer is defined as either June-August (JJA) or
470 July-September (JAS), and Northern Hemisphere winter is defined as either December-February
471 (DJF) or January-March (JFM); and vice versa for Southern Hemisphere summer/winter. ~~As briefly~~
472 introduced in Section 1, Using atmospheric diagnostics, the ~~the~~ focus is on ~~three~~ two separate
473 measures: i) to describe and understand the differences between the ~~current~~ two most recent two
474 warm climate simulations and the *piControl* in terms of temperature, rainfall and atmospheric/oceanic
475 circulation changes; and ii) to compare both current simulations, as well as simulations from previous
476 versions of the UK model (where available), with existing and the aforementioned newly-available
477 proxy data, to assess any improvements due to model advances. A final aim, discussed only briefly
478 here but shown in the Supplementary Material, is to include previous CMIP5 models to address the
479 question of whether any of the simulations produce enough rainfall to allow vegetation growth across
480 the Sahara: the mid-Holocene ‘Saharan greening’ and iii) ~~to compare both current simulations with~~
481 ~~those from previous versions of the UK model (where available), such as HadGEM2-ES or HadCM3,~~
482 ~~in order to assess any improvements due to model advances. In this aim, previous CMIP3 and 5~~
483 ~~versions of the UK model, alongside other CMIP5 models, will be assessed to address the question of~~
484 ~~whether simulations produce enough rainfall to allow vegetation growth across the Sahara: the mid-~~
485 ~~Holocene ‘Saharan greening’ problem.~~

486

487 **3.21.1. Do the CMIP6 HadGEM3 warm climate simulations show temperature, rainfall and**
488 **atmospheric/oceanic circulation differences when compared to the pre-industrial era?**

489 Here we focus on mean differences between the HadGEM3 warm climate simulations and the
490 corresponding *piControl*. Calendar adjusted Seasonal annual and seasonal mean summer-~~and~~/winter
491 1.5 m air temperature anomalies (relative to the *piControl*) from both warm climate simulations are
492 shown in Figure 2.– As an example and for comparative purposes, the same figure but where the data
493 are based on the modern calendar is shown in the Supplementary Material (SM5); this suggests that
494 the impact of the calendar adjustments on this field, and at this spatial and temporal scale, is
495 negligible, with the only obvious impact occurring over the Northern Hemisphere polar regions
496 during JJA in both simulations, but more so in the *lig127k* simulation (due to the larger changes in
497 insolation resulting in a larger change to the calendar, relative to the MH). Consistent with the
498 seasonality of the changes, the differences between either simulations are less at the annual timescale
499 (Figure 2a and d) than during individual seasons, but are still nevertheless to statistically significant at
500 the 99% level. During JJA, the *midHolocene* is showing a widespread statistically significant increase
501 in temperatures of up to 2°C across the entire Northern Hemisphere north of 30°N, more in some
502 places e.g. Greenland (Figure 2b), consistent with the increased latitudinal and seasonal distribution of
503 insolation caused by known differences in the Earth’s axial tilt (Berger & Loutre 1991, Otto-Bliesner
504 *et al.* 2017). The only places showing a reduction in temperature are West and ~~central~~Central Africa
505 (around 10°N) and northern India; this, as discussed below, is likely related to increased rainfall in
506 response to a stronger summer monsoon, but could also be due to the resulting increase in cloud cover
507 (reflecting more insolation) or a combination of the two. During DJF, only the Northern Hemisphere
508 high latitudes (north of 60°N) continue this warming trend, with the rest of continental Africa and
509 Asia showing a reduction in temperature (Figure 2c). These patterns are virtually the same-during in
510 the *lig127k* simulation (Figure 2e and f), just much more pronounced (with statistically significant
511 temperature increases during JJA of 5°C or more); again, this is consistent with the differences in the
512 Earth's axial tilt, which were more extreme (and therefore Northern Hemisphere summer experienced
513 larger insolation changes) in the LIG relative to the MH (Berger & Loutre 1991, Otto-Bliesner *et al.*
514 2017). Another clear feature of these figures, at either annual or seasonal timescales, is polar
515 amplification, which is likely associated with changes in sea-ice; as shown in the Supplementary
516 Material (SM6), statistically significant decreases in sea-ice are shown throughout the polar regions of
517 both hemispheres in the *midHolocene*, relative to the *piControl*. The same is true for the *lig127k*
518 simulation, just more pronounced (not shown).

519
520 Calendar adjusted seasonal mean summer and winter surface daily rainfall anomalies (again relative
521 to the *piControl*) from both warm climate simulations are shown in Figure 3. In line with the
522 aforementioned increased latitudinal and seasonal distribution of insolation, the largest differences in
523 either simulation occur during Northern Hemisphere summer (Figure 3b and e). Both warm climate

524 simulations are showing statistically against increases in rainfall around the monsoon regions,
525 especially over northern India and equatorial Africa, more so in the *lig127k* (Figure 3e). Both
526 simulations are also showing oceanic drying relative to the *piControl*, especially in the equatorial
527 Atlantic and Pacific, again more pronounced in the *lig127k* (Figure 3e). In contrast, during DJF, less
528 of an impact is seen in either simulation relative to the *piControl*, with a small but statistically
529 significant increase in rainfall in oceanic equatorial regions but drying over tropical land regions e.g.
530 southern Africa, central Brazil and northern Australia (Figure 3c and f). Again, consistent with the
531 increased insolation changes during the LIG compared to the MH, these differences are stronger in the
532 *lig127k* simulation (Figure 3f). Consistent with the temperature differences, these signals are again
533 weaker at the annual timescale but are nevertheless statistically significant (Figure 3a and b).

534

535 A measure of oceanic circulation is also considered here, shown by the three HadGEM3 simulations
536 of meridional overturning circulation (MOC) in the Atlantic basin and globally (Figure 4a-c and d-f,
537 respectively). Although not identical, the differences are nevertheless negligible, with both warm
538 climate simulations almost exactly reproducing the structures of weakly and strongly overturning
539 MOC seen in the *piControl*; for example, the strongly overturning MOC in the upper levels of the
540 Atlantic is marginally stronger in the *midHolocene* at ~30-40°N relative to the other two simulations,
541 but the structures are very similar. This suggests that the changes to atmospheric fields such as P-E,
542 energy fluxes and wind stress (in response to the insolation changes) are having a minimal impact on
543 the overturning circulation, and this is consistent with other work (e.g. Guarino *et al.* [2020]).

544

545 A key region of interest, concerning mean precipitation changes and changes to the extent and
546 latitudinal distribution of monsoon regions, is northern Africa, primarily because of the
547 mentioned inability of previous models to reproduce the increases shown by the proxy data here
548 (e.g. Braconnot *et al.* 2007, Braconnot *et al.* 2012). Therefore, Figure 5 reproduces the above
549 precipitation changes but zooms into Africa and additionally includes Mean-calendar adjusted mean
550 JJA (the primary monsoon region) rainfall and 850mb wind anomalies (relative to the *piControl*) from
551 both warm climate simulations are shown in Fig_wafricanrain_prod, which zooms into Africa. In
552 response to the increased Northern Hemisphere summer insolation, the West African monsoon is
553 enhanced in both simulations, with positive (negative) rainfall anomalies across sub-Saharan Africa
554 (eastern equatorial Atlantic) suggesting a northward displacement of the ITCZ rainfall maxima. This
555 is consistent with previous work, with a northward movement of the rainbelt being associated with
556 increased advection of moisture into the continent (Huang *et al.* 2001, Singarayer *et al.* 2017, Wang *et*
557 *al.* 2014). This increased advection of moisture is shown by the enhanced low-level westerlies at all
558 latitudes but especially over the regions of rainfall maxima in Figure 5a and b Fig_wafricanrain_prod,
559 drawing in more moisture from the tropical Atlantic, which are consistent with previous work
560 documenting the intensified monsoon circulation associated with a greater land-sea temperature

561 ~~contrast~~ (Huang *et al.* 2001, Singarayer *et al.* 2017, Wang *et al.* 2006). This pattern is enhanced in the
562 *lig127k* relative to the *midHolocene*, again in response to the stronger insolation changes relative to
563 the MH, and the northward displacement of the ~~ITCZ~~ central rainbelt is more pronounced in the
564 *lig127k* simulation (Figure 5 Fig_wafricanrain_prod c). ~~Interestingly, however, regarding very small~~
565 ~~anomalies (i.e. $< 1 \text{ mm day}^{-1}$), the *midHolocene* is showing wetter conditions further north,~~
566 ~~throughout the Sahara and up to the Mediterranean, whereas the *lig127k* simulation has small dry~~
567 ~~anomalies in this region (Fig_wafricanrain_prod a and b for the *midHolocene* and *lig127k*,~~
568 ~~respectively).~~

569

570 The change to the intensity and the spatial pattern (e.g. latitudinal positioning and extent) of the West
571 African monsoon is further shown in Figure 6, which shows calendar adjusted daily JJA rainfall by
572 latitude over West Africa (averaged over 20°W-15°E, land points only) from both warm climate
573 simulations. This figure also includes MH and LIG simulations from previous generations of the
574 same model. It should be noted that although LIG experiments have been conducted previously with
575 both model-model and model-data comparisons being made (Lunt *et al.* 2013), all of these
576 experiments were carried out using early versions of the models and were thus not included in
577 CMIP5. Moreover, as part of their assessment Lunt *et al.* (2013) considered a set of four simulations,
578 at 130, 128, 125 and 115 ka, none of which are directly comparable to the current HadGEM3 *lig127k*
579 simulation. Instead, a LIG simulation has recently been undertaken using one of the original versions
580 of the UK's physical climate model, HadCM3, and so this is used here to compare with the *lig127k*
581 simulation.

582

583 Beginning with the recent paleoclimate HadGEM3 simulations, in line with the changes in insolation
584 both warm climate simulations are showing higher absolute values at their peak (between $\sim 7.5\text{-}10^\circ\text{N}$)
585 than the *piControl* (Figure 6a). Concerning anomalies, both simulations are showing a large increase
586 in rainfall relative to the *piControl* (of ~ 2 and 6 mm day^{-1} for the *midHolocene* and *lig127k*,
587 respectively) over the monsoon region between $\sim 10\text{-}12^\circ\text{N}$ (Figure 6b). Relative to previous versions
588 of the same model, the previous generation (HadGEM2-ES) is slightly drier than HadGEM3 over this
589 region for its PI simulation and slightly wetter for its MH simulation; conversely, the version before
590 that (HadCM3) is consistently wetter than HadGEM3, for all of its simulations (Figure 6a). There
591 also appears to be a northward displacement in the oldest version, with the largest difference between
592 the simulations and their corresponding PI simulations occurring at $\sim 11^\circ\text{N}$ in the two most recent
593 versions of the model, whereas in HadCM3 this appears to be shifted northwards to $\sim 12.5^\circ\text{N}$ (Figure
594 6b). This northward displacement in certain models consistent with previous work (e.g. Huang *et al.*
595 2001, Otto-Bliesner *et al.* 2017, Singarayer *et al.* 2017, Wang *et al.* 2014). In terms of the latitudinal
596 extent, the results suggest that all warm climate simulations (regardless of generation) are producing a
597 wider Northern Hemisphere monsoon region (i.e. a greater northerly extent) relative to each version's

598 [PI, with rainfall falling to near zero at ~18°N in the PI simulations but extending to 20°N \(and above,](#)
599 [in terms of the LIG simulations\) in both warm climate simulations \(Figure 6a\). This is again](#)
600 [consistent with previous work, where various theories are compared as to the reasons behind the](#)
601 [latitudinal changes in the rainbelt's position, one which is a symmetric expansion during boreal](#)
602 [summer \(Singarayer & Burrough 2015, Singarayer et al. 2017\).](#)

603
604 **3.21.2. Model- Simulation comparison and Model-Data comparison: Do the CMIP6 HadGEM3**
605 **simulations reproduce the ‘reconstructed’ climate based on available proxy data, and has there**
606 **been any noticeable improvement relative to previous versions of the same model?**

607 [Although the above analysis is useful and confirms that the most recent warm climate simulations are](#)
608 [responding consistently to the increased latitudinal and seasonal distribution of insolation, it does not](#)
609 [give any information on which \(if any\) of the simulations is most accurate or which version of the](#)
610 [model is better at reproducing proxy-observed conditions. Therefore, here we focus on bring in a](#)
611 [comparison with newly-available recent proxy data, comparing these to all versions of the model,](#)
612 [focusing on surface air temperature, SST and rainfall \(drawing direct comparisons, as well as using](#)
613 [the root mean square error \(RMSE\) but without a cut-off threshold\), between both proxy and vs](#)
614 [simulated data and HadGEM3 vs previous versions, summarised in Table 4a\).](#) The aim of this is to
615 [firstly to see how well the current warm climate simulations are reproducing the ‘observed’](#)
616 [approximate magnitudes and patterns of change, and secondly to assess any possible improvement](#)
617 [from previous versions of the same model.](#) It is worth noting that both simulated and proxy anomalies
618 contain a high level of uncertainty [\(as measured by the standard deviation\)](#), and in many locations the
619 uncertainty is ~~often~~ larger than the anomalies themselves (not shown). The following results should
620 therefore be considered with this caveat in mind.

621
622 Before the spatial patterns are compared, it is useful to assess global means [from the three HadGEM3](#)
623 [simulations](#) (focusing on 1.5 m air temperature, calculated both annually and during Northern and
624 Southern Hemisphere summer, JJA and DJF respectively) ~~for model-model comparisons~~. Table 3
625 shows these global means, where it is clear that when annual means are considered, the *midHolocene*
626 simulation is actually cooler than the *piControl*. This discrepancy with the palaeodata, which ~~is~~
627 [general at many locations](#) suggests a warmer MH relative to PI, [and this is consistent with previous](#)
628 [work using other models \(e.g. also exists in previous models, and is termed the ‘Holocene temperature](#)
629 [conundrum’ by Lui et al. \(2014\).](#) The *lig127k* simulation is, however, warmer than the *piControl*
630 simulation. Given the seasonal distribution of insolation in these two simulations, it is expected that
631 the largest difference to the *piControl* occurs during boreal summer, and indeed it does; during JJA,
632 there is a warmer *lig127k* and a slightly warmer *midHolocene* (1.69°C and 0.07°C, respectively). The
633 opposite is true during DJF.

634

635 Concerning the spatial patterns during the MH, Fig_proxy_mh_loc shows simulated surface MAT and
636 MAP anomalies from the *midHolocene* simulation versus MH proxy anomalies from Bartlein *et al.*
637 (2011), both of which have over 600 proxy locations in total (Table 4), although mostly confined to
638 the Northern Hemisphere. For MAT, globally the simulation looks reasonable (RMSE = 2.45°C), and
639 appears to be able to reproduce the sign of temperature change for many locations, with both
640 simulated and proxy anomalies suggesting increases in temperature North of 30°N
641 (Fig_proxy_mh_loc a and b). This is not true everywhere, such as across the Mediterranean where
642 the simulation suggests a small warming but the proxy data indicates cooling (Fig_proxy_mh_loc a
643 and b). However, regarding the magnitude of change, the *midHolocene* simulation is underestimating
644 the temperature increase across most of the Northern Hemisphere, with for example increases of up to
645 1°C across Europe from the simulation compared to 3–4°C increases from the proxy data
646 (Fig_proxy_mh_loc a and b). In the simulation, temperature anomalies only reach these magnitudes
647 in the Northern Hemisphere polar region (i.e. north of 70°N), not elsewhere. A similar conclusion can
648 be drawn from MAP (RMSE = 280 mm yr⁻¹), where again the *midHolocene* simulation is correctly
649 reproducing the sign of change across most of the Northern Hemisphere, but in some places not the
650 magnitude. Over the eastern US, for example, rainfall decreases of up to 200 mm yr⁻¹ are being
651 shown by the simulation whereas the proxy data suggests a much stronger drying of up to 400 mm yr⁻¹
652 (Fig_proxy_mh_loc c and d). Elsewhere, such as over Europe and Northern Hemisphere Africa, the
653 simulation more accurately reproduces the magnitude of rainfall increases; both simulated and proxy
654 anomalies show increases of 200–400 mm yr⁻¹ (Fig_proxy_mh_loc c and d).

655
656 Concerning the spatial patterns during the MH, Figure 7 shows simulated surface MAT anomalies
657 from the current *midHolocene* simulation and those from two previous versions of the same model,
658 versus MH proxy anomalies from Bartlein *et al.* (2011). Note that, here, statistical significance of the
659 simulated anomalies has not been shown, because firstly the aim here is to assess all differences
660 regardless of significance and secondly because a measure of statistical significance (for HadGEM3)
661 has already been presented in Figure 2; statistical significance from the other versions of the same
662 model is virtually identical (not shown). Globally, all three models are showing a reasonable level of
663 agreement to the proxy data, with RMSE = 2.45°C, 2.42°C and 2.37°C for HadGEM3, HadGEM2-ES
664 and HadCM3, respectively (Table 4a). Using this metric, the oldest version of the model (HadCM3)
665 is doing marginally better than the other models, relative to the proxy data. Spatially, however, there
666 are differences to the proxy data and between model generations. Although all three generations
667 appear to be able to reproduce the sign of temperature change for many locations, with both simulated
668 and proxy anomalies suggesting increases in temperature North of 30°N and especially over northern
669 Europe, the Arctic Circle increases are not as homogenous in HadCM3 (Figure 7d) and indeed this
670 model shows cooling over the Greenland Sea. Although this cannot be corroborated by the proxy
671 data, due to a lack of coverage, neither of the later generation models show this to the same extent

672 (Figure 7b and c). Discrepancies with the proxy data also occur in all three simulations across the
673 Mediterranean region, where all three simulations suggest a small warming but the proxy data
674 indicates cooling (Figure 7). Moreover, regarding the magnitude of change, all three simulations are
675 underestimating the temperature increase across most of the Northern Hemisphere, with for example
676 increases of up to 1°C across Europe from the simulations compared to 3-4°C increases from the
677 proxy data. In the simulations, temperature anomalies only reach these magnitudes in the Northern
678 Hemisphere polar region (i.e. north of 70°N), not elsewhere. Further equatorward, all three
679 simulations are identifying a slight cooling over the West African monsoon region (as discussed
680 above), but the accuracy of this relative to the proxy data is difficult to ascertain given the lack of
681 coverage across Africa and, where there are data locations, a highly variable sign of change (Figure
682 7a).

683
684 A similar conclusion can be drawn from MAP, shown in Figure 8, where all three simulations are
685 correctly reproducing the sign of change across most of the Northern Hemisphere, although more so
686 in the two most recent generations of the model (HadGEM3 and HadGEM2-ES), but in some places
687 not the magnitude. Over the eastern US, for example, rainfall decreases of up to 200 mm yr⁻¹ are
688 being shown by the simulations (Figure 8b-d) whereas the proxy data suggests a much stronger drying
689 of up to 400 mm yr⁻¹ (Figure 8a). Elsewhere, such as over Europe and Northern Hemisphere Africa,
690 the simulations more accurately reproduce the magnitude of rainfall increases; both simulated and
691 proxy anomalies show increases of 200-400 mm yr⁻¹. Globally, Table 4a suggests that the most recent
692 generation model, HadGEM3, is doing better than the others, relative to the proxy data (RMSE =
693 285.9 mm yr⁻¹, 293.5 mm yr⁻¹ and 304.7 mm yr⁻¹ for HadGEM3, HadGEM2-ES and HadCM3,
694 respectively). In terms of how the spatial patterns change according to model version, during the MH
695 the two most recent simulations generally agree (RMSE = 90.8 mm year⁻¹, Table 4a) and show similar
696 spatial patterns; focusing again on the African monsoon region (for the aforementioned reasons), both
697 simulations show a drier equatorial Atlantic during the MH and then increased rainfall around 10°N
698 (Figure 8b and c for HadGEM3 and HadGEM2-ES, respectively). Both simulations also suggest that
699 the increases in rainfall extend longitudinally across the entire African continent, with the largest
700 changes not only occurring across western and central regions but also further east. In contrast,
701 globally HadCM3 agrees less with HadGEM3 (RMSE = 121.8 mm year⁻¹, Table 4a) and only
702 suggests a wetter MH over West Africa, not further east. HadCM3, and indeed HadGEM2-ES, also
703 differs from the most recent simulation over the equatorial Atlantic, showing a region of drying that is
704 not only stronger in magnitude but also larger in terms of spatial extent; whilst still present in
705 HadGEM3, this feature that is much weaker (Figure 8b-d).

706

707 Concerning the spatial patterns during the LIG, Fig8_proxy_lig_loc shows simulated mean SST
708 anomalies (calculated both annually and during JAS/JFM) from the lig127k simulation and LIG proxy

709 anomalies from two sources, Capron *et al.* (2017) and Hoffman *et al.* (2017). When annual anomalies
710 are considered, despite the lack of reconstructions in the Capron *et al.* (2017) data (Table 4), there is
711 relatively good agreement (RMSE = 2.44°C and 2.94°C for the Capron *et al.* (2017) and Hoffman *et*
712 *al.* (2017) data, respectively, and which is within the average uncertainty range), between simulated
713 and observed SST anomalies in the Northern Hemisphere (and in particular in the North Atlantic),
714 with both suggesting increased temperatures during the LIG of up to 3°C (Fig_proxy_lig_loc a).
715 There are discrepancies, such as in the Norwegian Sea, where the Hoffman *et al.* (2017)
716 reconstructions suggest a cooler LIG than preindustrial, whereas the *lig127k* simulation shows a
717 consistent warming; this is, however, consistent with previous work, and earlier climate models have
718 also failed to capture this cooling (Capron *et al.* 2014, Stone *et al.* 2016). Note that, over Greenland
719 and Antarctica, the Capron *et al.* (2017) proxy data show SAT, not SST, and are therefore not
720 compared in this figure; comparison with simulated SAT, however, suggests that the model is
721 capturing the sign, if not the magnitude, of annual change over these regions (not shown). During
722 Northern Hemisphere summer, JAS (during which period Capron *et al.* [2017] has the most proxy
723 locations [Table 4]), the simulated anomalies are in agreement with many, but not all, of the proxy
724 locations (RMSE = 3.11°C and 2.06°C for the Capron *et al.* (2017) and Hoffman *et al.* (2017) data,
725 respectively); examples of where they differ, not just in magnitude but also sign, again include the
726 Norwegian and Labrador Seas (Fig_proxy_lig_loc b). In Southern Hemisphere summer, JFM, the
727 model suggests a general (but weak) cooling in the South Atlantic relative to preindustrial and a
728 general (but weak) warming in the Southern Ocean (Fig_proxy_lig_loc c). However, certain proxy
729 locations (such as off the coast of southern Africa) suggest a much warmer LIG than preindustrial
730 (RMSE = 1.94°C and 4.24°C for the Capron *et al.* (2017) and Hoffman *et al.* (2017) data,
731 respectively), which in stark contrast to the cooling in the same region from the *lig127k* simulation
732 (Fig_proxy_lig_loc c). In the Southern Ocean, the majority of simulated anomalies reproduce the
733 observed sign of change, but not the magnitude; the *lig127k* simulation suggests temperature increases
734 of up to 1°C, whereas both proxy datasets suggest SST increases of 2–3°C depending on location
735 (Fig_proxy_lig_loc e).

736

737 Concerning the spatial patterns during the LIG, Figure 9 shows simulated mean SST anomalies
738 (calculated both annually and during JAS/JFM) from the current *lig127k* simulation and that from the
739 oldest version of the same model, versus LIG proxy anomalies from two sources, Capron *et al.* (2017)
740 and Hoffman *et al.* (2017). No LIG simulation using HadGEM2-ES is currently available. When
741 annual anomalies are considered, there is relatively good agreement globally between HadGEM3 and
742 the proxy data where RMSE = 3.03°C and 2.42°C for the Capron *et al.* (2017) and Hoffman *et al.*
743 (2017) data, respectively (Table 4b). HadCM3 performs marginally better when compared to the
744 Capron *et al.* (2017) data, but worse when compared to the Hoffman *et al.* (2017) data (Table 4b).
745 Similarly varying results also occur when JAS and JFM anomalies are considered, with HadGEM3

746 comparing slightly better or worse than HadCM3 according to season and proxy dataset used; all of
747 the values, however, show relatively good agreement, with no simulation exceeding RMSE = 4.5°C in
748 any season or with any dataset (Table 4b). Spatially, HadGEM3 is showing a general agreement
749 between simulated and proxy annual and JAS anomalies in the Northern Hemisphere (and in
750 particular in the North Atlantic), with both suggesting increased temperatures during the LIG of up to
751 5°C (Figure 9a and b). HadCM3 is not capturing these magnitudes at the annual timescale (Figure 9d)
752 and, despite showing greater warming during JAS, is still lower than HadGEM3; this is more in
753 agreement with the proxy data at higher latitudes (e.g. the western Norwegian Sea at ~70°N) but less
754 so further south (Figure 9e). This might suggest that, in this region, HadGEM3 is actually
755 overestimating the degree of warming. Nevertheless, in both versions of the model there are
756 discrepancies concerning not just in the magnitude but also in the sign of change, such as in the
757 eastern Norwegian Sea or the Labrador Sea, where reconstructions suggest a cooler LIG but both
758 versions show a consistent warming (Figure 9b and e). This is, however, consistent with previous
759 work, and earlier climate models have also failed to capture this cooling (Capron *et al.* 2014, Stone *et*
760 *al.* 2016). In Southern Hemisphere summer, JFM, both versions agree on a general (but weak)
761 cooling in the South Atlantic relative to preindustrial and a weak warming in the Southern Ocean
762 (Figure 9c and f). In contrast certain proxy locations (such as off the coast of southern Africa) suggest
763 a much warmer LIG than preindustrial, which is opposite to the simulated cooling in the same region
764 (Figure 9c and f). Further south, the majority of simulated anomalies reproduce the observed sign of
765 change, but not the magnitude; here, the simulations suggest temperature increases of up to 1°C,
766 whereas both proxy datasets suggest SST increases of 2-3°C depending on location (Figure 9c and f).
767
768 For rainfall changes during the LIG, Figure 10 shows simulated annual mean surface rainfall
769 anomalies from the current *lig127k* simulation and that from the oldest version of the same model,
770 versus LIG proxy anomalies from Scusscolini *et al.* (2019). Note that the simulated anomalies shown
771 here are annual anomalies, as opposed to daily anomalies in Figure 3, to be consistent with the proxy
772 data. Note also that, for these proxy reconstructions, a semi-quantitative scale is used by Scusscolini
773 *et al.* (2019) rather than actual anomalies and is therefore reproduced here; this ranges from a unitless
774 -2 to 2, corresponding to ‘Much wetter LIG anomaly’, ‘Wetter’, ‘No noticeable anomaly’, ‘Drier’ and
775 ‘Much drier LIG anomaly’. It is for this reason that RMSE values have not been calculated here. As
776 was suggested from the MH simulations (Figure 8), both versions of the model are showing similar
777 patterns of rainfall changes, along the same lines as those seen during the MH but again enhanced
778 (Figure 10). Both versions are showing enhanced rainfall across the Northern Hemisphere equatorial
779 zone and in particular the monsoon regions during the LIG, often exceeding 500 mm year⁻¹ in some
780 places. In the Northern Hemisphere, both versions of the model are generally in agreement with the
781 proxy data, with most proxy locations showing ‘Wetter’ or ‘Much wetter’ conditions. There are,
782 however, some discrepancies elsewhere, such as the regions of tropical drying over e.g. Brazil and

783 southern Africa in the simulations being in stark contrast to the ‘Wetter’ conditions suggested by the
784 proxy data (Figure 10). Concerning the differences in the spatial patterns between the model versions,
785 although both generations qualitatively show similar patterns, there are subtle differences. Again
786 focusing on the African monsoon region, HadGEM3 shows greatly increased rainfall across all of
787 sub-Saharan Africa, centred on 10°N but extending from ~5°N to almost 20°N and longitudinally
788 across the entire African continent (Figure 10a). In contrast, and similar to the MH results, in
789 HadCM3 the largest rainfall increases are less apparent over East Africa (Figure 10b).

790

791 It would therefore be reasonable to say that, for both ~~warm climate~~ MH and LIG simulations, whilst
792 the most recent version of the model is capturing the sign and magnitude of change relative to proxy
793 reconstructions (for either temperature or rainfall) in some locations, this is highly geographically
794 dependent and there are locations where the current simulation fails to capture even the sign of
795 change. Compared to previous versions of the same model, any improvement also appears to be
796 highly variable according to metric, proxy reconstruction used for comparison and geographical
797 location, with for example HadGEM3 showing some improvement relative to previous versions for
798 rainfall during the MH, but not surface air temperature. The accuracy of the most recent ~~The~~ model,
799 and indeed previous generations, also appears to be seasonally dependent, with the most recent
800 lig127k simulation (~~but not the midHolocene simulation~~) correctly reproducing both the sign and
801 magnitude of change during Northern Hemisphere summer in some locations, but not during Southern
802 Hemisphere summer or annually. It would also appear that, for both the MH and LIG simulations,
803 whilst there is less difference between the most recent two configurations of the model, they are
804 nevertheless quite different to the oldest version. For global mean annual rainfall during the MH,
805 Table 4a shows a linear progression of improvement across the three versions of the model, as well as
806 more agreement between the two most recent model generations. This is also true when just the
807 region of rainfall maxima in northern Africa is considered, with both of the two most recent
808 generations, and especially HadGEM2-ES, being marginally closer to the proxy data than HadCM3
809 (RMSE = 463.7 mm yr⁻¹, 424.5 mm yr⁻¹ and 468.4 mm yr⁻¹ for HadGEM3, HadGEM2-ES and
810 HadCM3, respectively). In all simulations, although spatial patterns of rainfall are similar, there are
811 discrepancies especially over the African monsoon region; the oldest version of the model, for
812 example, only shows rainfall increases over West Africa, whereas the two most recent versions imply
813 Africa-wide rainfall increases at this latitude. If a comparison is made with satellite-derived rainfall
814 data for the modern West African monsoon (not shown), results suggest that rainfall maxima are not
815 just limited to West Africa but also occur over the central region and East Africa, more consistent
816 with the two most recent versions of the model. One reason for HadCM3 not identifying this
817 longitudinal extent might be connected to the very coarse spatial resolution of this model, relative to
818 the others, impacting any topographically-induced rainfall, especially over the East African
819 Highlands.

820

821 **3.2.3. Model-Model comparison: Do the CMIP6 HadGEM3 simulations show an improvement**
822 **compared to older CMIP versions of the UK model?**

823 Here we focus on model-model intercomparisons, comparing the HadGEM3 warm climate
824 simulations with firstly those from previous versions of the UK model and secondly with those from
825 other models included in CMIP5. It should be noted that although LIG experiments have been
826 conducted previously with both model-model and model-data comparisons being made (Lunt *et al.*
827 2013), all of these experiments were carried out using early versions of the models and were thus not
828 included in CMIP5. Moreover, as part of their assessment Lunt *et al.* (2013) considered a set of four
829 simulations, at 130, 128, 125 and 115 ka, none of which are directly comparable to the current
830 HadGEM3 *lig127k* simulation. Instead, a LIG simulation has recently been undertaken using one of
831 the original versions of the UK's physical climate model, HadCM3, and so this is used here to
832 compare with the *lig127k* simulation. As discussed above, this section is divided into two parts:
833 firstly the mean climate state of the warm climate simulations will be compared to the model's
834 predecessors, focusing again on hydroclimate of the West African monsoon (given the known
835 problem of simulated rainfall underestimation in this region, see e.g. Braconnot *et al.* [2007]). Here,
836 both direct comparisons and RMSE values will again be examined, this time calculating the RMSE
837 between the simulated rainfall anomaly from two older versions of the UK model versus the current
838 HadGEM3 *midHolocene* and *lig127k* simulations (summarised in Table 4b).

839

840 Secondly, previous generation simulations (from all available models included in CMIP5) will be
841 compared to see whether the most recent HadGEM3 *midHolocene* simulation is now providing
842 enough rainfall to allow vegetation growth across the Sahara; something which previous generations
843 of models from CMIP5 did not (Braconnot *et al.* 2007).

844

845 **3.2.3.1. Mean climate state from predecessors of HadGEM3**

846 Regarding the magnitude and latitudinal extent of the West African monsoon, Fig_latrain_gen shows
847 the JJA rainfall differences averaged over West Africa from the current *midHolocene* and *lig127k*
848 simulation versus two of the model's predecessors. During the MH, the two most recent generations
849 of the model (HadGEM3 and HadGEM2-ES) generally agree on drier conditions over the equatorial
850 Atlantic and then wetter conditions over West Africa, however the oldest generation model
851 (HadCM3) does not reproduce the Atlantic drying. Likewise the two most recent generations share a
852 similar latitudinal distribution of rainfall above $\sim 5^{\circ}\text{N}$, with a wetter MH over land, peaking at $\sim 2-3$
853 mm day^{-1} at $\sim 11-12^{\circ}\text{N}$. Interestingly, the previous version of the model (HadGEM2-ES) shows the
854 strongest and most northwardly displaced rainfall peak, as discussed in previous work (e.g. Huang *et al.*
855 2001, Otto-Bliesner *et al.* 2017, Singarayer *et al.* 2017, Wang *et al.* 2014); the most recent version,
856 HadGEM3, has lower northward displacement compared to the two older versions of the model. Both

857 recent versions suggest that the monsoon region extends to $\sim 17^{\circ}\text{N}$, above which the differences
858 between the MH and PI reduce to near zero. In contrast, HadCM3 suggests a generally weaker, but
859 latitudinally more extensive, monsoon region, suggesting a wetter MH (by $\sim 1\text{ mm day}^{-1}$) as far north
860 as 20°N and beyond. For the LIG, HadGEM3 is showing a much stronger monsoon region relative to
861 the *piControl*, compared to HadCM3. However, in terms of extent, similar results are shown to those
862 for the MH, with HadCM3 showing a generally weaker, but more northwardly displaced, monsoon
863 region. In this older generation model, positive rainfall anomalies of $\sim 2\text{--}3\text{ mm day}^{-1}$ extend as far
864 north as $17\text{--}18^{\circ}\text{N}$, whereas in HadGEM3 they fall to $\sim 1\text{ mm day}^{-1}$ at these latitudes.

865

866 In terms of the spatial patterns of the West African monsoon, Fig_wafricanrain_gen_mh and
867 Fig_wafricanrain_gen_lig show the JJA daily rainfall climatology differences from the same three
868 model generations for the MH and LIG, respectively. During the MH, consistent with
869 Fig_latrain_gen, the two most recent simulations generally agree (RMSE = 0.46 mm day^{-1}) and show
870 similar spatial patterns, with a drier equatorial Atlantic during the MH and then increased rainfall
871 around 10°N (Fig_wafricanrain_gen_mh a and b for HadGEM3 and HadGEM2-ES, respectively).
872 Both simulations also suggest that the increases in rainfall extend longitudinally across the entire
873 continent, with the largest changes not only occurring across western and central regions but also
874 further east. In contrast, HadCM3 is less consistent than HadGEM3 (RMSE = 0.53 mm day^{-1}) and
875 only suggests a wetter MH over West Africa; moreover, again consistent with Fig_latrain_gen,
876 HadCM3 suggests that although the West African monsoon region is longitudinally narrower, it is
877 latitudinally wider than the other two simulations (Fig_wafricanrain_gen_mh c). HadCM3 also differs
878 from the other simulations over the equatorial Atlantic, showing a region of drying that is not only
879 stronger in magnitude (with the MH being over 5 mm day^{-1} drier than the PI in HadCM3, compared to
880 $\sim 2\text{--}3\text{ mm day}^{-1}$ in the two most recent simulations), but also larger in terms of latitude and longitude
881 extent (Fig_wafricanrain_gen_mh e).

882

883 During the LIG, only the most recent and oldest version of the model can be compared, as a LIG
884 simulation using HadGEM2-ES is unavailable. In Fig_wafricanrain_gen_lig there is a noticeable
885 difference between generations and the level of agreement is the lowest across all simulation
886 combinations (RMSE = 1.57 mm day^{-1}), with the most recent HadGEM3 showing greatly increased
887 rainfall across all of northern Africa, centred on 10°N but extending from $\sim 5^{\circ}\text{N}$ to almost 20°N and
888 beyond (Fig_wafricanrain_gen_lig a), again consistent with Fig_latrain_gen. In contrast, and similar to
889 the MH results, in HadCM3 the largest rainfall increases are confined to Western Africa only, rather
890 than extending longitudinally across the continent (Fig_wafricanrain_gen_lig b). However, in terms of
891 latitudinal extent, HadCM3 is showing weak wet anomalies all the way to the Mediterranean, whereas
892 the monsoon region diminishes further south (at $\sim 30^{\circ}\text{N}$) in HadCM3 and dry anomalies are suggested
893 North of this. Another noticeable difference is the region of drying, with the most recent generation

894 ~~model placing this over the equatorial Atlantic (consistent with the MH) but HadCM3 shifting this~~
895 ~~further east, over most of central Africa (Fig_wafricanrain_gen_lig b). The region of equatorial~~
896 ~~Atlantic drying shown by the more recent versions of the model is actually wetter during this~~
897 ~~HadCM3 LIG simulation.~~

898

899 ~~It would therefore appear that, for the MH, whilst there is less difference between the most recent two~~
900 ~~configurations of the model (in terms of a more localised West African monsoon region), there~~
901 ~~nevertheless has been improvement since the oldest version of the UK's physical climate model. For~~
902 ~~the LIG, where unfortunately there is no intermediate generation, it would be reasonable to say that~~
903 ~~again considerable change has occurred since the oldest generation model, with the suggestion that,~~
904 ~~although HadCM3 is identifying an enhanced monsoon which extends to the Mediterranean (albeit~~
905 ~~with very weak anomalies), at lower latitudes it is not showing the level of northward displacement as~~
906 ~~the most recent version, apart from in the far western regions.~~

907

908 **3.21.3. Rainfall across the Saharan greening**

909 Finally, a brief discussion is given on the 'Saharan greening' question. Given that the warm climate
910 simulations, and indeed the *piControl*, did not use interactive, ~~but rather prescribed,~~ vegetation, it is
911 not possible to directly test if the model is reproducing the 'Saharan greening'² that proxy data suggest.
912 For example, Jolly *et al.* (1998a, 1998b) analysed MH pollen assemblages across northern Africa and
913 suggested that some areas south of 23°N (characterised by desert today) were grassland and
914 xerophytic woodland/scrubland during the MH (Joussaume *et al.* 1999). To circumvent this caveat,
915 Joussaume *et al.* (1999) developed a method for indirectly assessing Saharan greening, based on the
916 annual mean rainfall anomaly relative to a given model's modern simulation. Using the water-
917 balance module from the BIOME3 equilibrium vegetation model (Haxeltine & Prentice 1996),
918 Joussaume *et al.* (1999) calculated the increase in mean annual rainfall, zonally averaged over 20°W-
919 30°E, required to support grassland at each latitude from 0 to 30°N, compared to the modern rainfall
920 at that latitude. This was then used to create maximum and minimum estimates, within which bounds
921 the model's annual mean rainfall anomaly must lie to suggest enough of an increase to support
922 grassland (Joussaume *et al.* 1999).

923

924 Therefore, an adapted version of Figure 3a in Joussaume *et al.* (1999) is shown in the Supplementary
925 Material (SM7), which shows mean annual rainfall anomalies by latitude (to be consistent with the
926 proxy data-based threshold) from not only the current *midHolocene* simulation, but also all previous
927 MH simulations from CMIP5. Concerning the threshold required to support grassland, it is clear that
928 although the current *midHolocene* simulation is just within the required bounds at lower latitudes (e.g.
929 up to 17°N), north of this the current *midHolocene* simulation is not meeting the required threshold,
930 neither are any of the other CMIP5 models after ~18°N (SM7). It would therefore appear that the

931 'Saharan greening' problem has yet to be resolved, and may well only be reproduced once interactive
932 vegetation, and indeed interactive dust, is included in the simulation; given the current lack of an
933 interactive vegetation/dust model, vegetation-related climate feedbacks (e.g. albedo) on the system are
934 therefore currently missing.

935

936 **4. SUMMARY AND CONCLUSIONS**

937 This study has conducted and assessed the mid-Holocene and Last Interglacial simulations using the
938 latest version of the UK's physical climate model, HadGEM3-GC3.1, comparing the results firstly
939 with the model's preindustrial simulation and secondly with previous versions the same model,
940 against with available proxy data, previous versions of the same model, and other models from
941 CMIP's previous iteration, CMIP5. – Therefore this study is novel, being the first time this version of
942 the UK model has been used to conduct any paleoclimate simulations and therefore the first time we
943 are in a position to include them as part of the UK's contribution to CMIP6/PMIP4. Both the
944 *midHolocene* and *lig127k* simulations followed the experimental design defined in Otto-Bliesner *et al.*
945 (2017) and under the auspices of and the CMIP6/PMIP4 protocol. – Both simulations were run for a
946 350-400 year spin-up phase, during which ~~time~~ atmospheric and oceanic equilibrium ~~was~~ were
947 assessed, and once an acceptable level of equilibrium had been reached, the production runs were
948 started.

949

950 Concerning the results from the spin-up phase, comparison to the metrics used to assess the CMIP6
951 piControl suggest that both warm climate simulations reached an acceptable state of equilibrium, in
952 the atmosphere at least, to allow the production runs to be undertaken. From these, both simulations
953 are showing global temperatures consistent with the latitudinal and seasonal distribution of insolation,
954 and with previous work (e.g. Otto-Bliesner *et al.* 2017). Globally, whilst both the recent simulations
955 are mostly capturing the sign and, in some places, magnitude of change relative to the PI, similar to
956 previous model simulations this is geographically and seasonally dependent. It should be noted that
957 the proxy data (against which the simulations are evaluated) also contain a high level of uncertainty in
958 both space and time (in terms of both seasons and geological era), and so it is encouraging that the
959 simulations are generally reproducing the large-scale sign of change, if not at an individual location.
960 Compared to previous versions of the same model, this appears to vary according to metric, proxy
961 reconstruction used for comparison and geographical location. In some instances, such as annual
962 mean rainfall in the MH, there is a clear and linear improvement (relative to proxy data) through the
963 model generations when rainfall is considered globally; likewise there is more accuracy in the two
964 recent versions (again relative to proxy data) than the oldest version when only the West African
965 monsoon region is considered (see Table 4a and the RMSE values discussed in the concluding
966 paragraph of Section 3.1.2).

968 Likewise, [when zooming into Africa](#), the behaviour of the West African monsoon in both [HadGEM3](#)
969 [warm climate](#) simulations is consistent with current understanding (e.g. Huang et al. 2001, Singarayer
970 et al. 2017, Wang et al. 2014), which suggests a wetter (and possibly latitudinally wider, and/or
971 northwardly displaced) monsoon during the MH and LIG, relative to the PI. Regarding model
972 development in simulating the West African monsoon, [there are differences between model](#)
973 [generations; the oldest version of the model, for example, limits the rainfall increases to over sub-](#)
974 [Saharan West Africa only, whereas the two most recent versions imply Africa-wide \(i.e. across all](#)
975 [longitudes\) rainfall increases at this same latitudea.](#) ~~Although there has been an improvement since~~
976 ~~the oldest version of the UK's physical climate model (HadCM3), the two most recent version of the~~
977 ~~model yield similar results in terms of both intensity and position.~~ Lastly, regarding the well-
978 documented ‘Saharan greening’ during the MH, results here suggest that the most recent version of
979 the UK’s physical climate model is consistent with all other previous models to date.

980

981 In conclusion, the results suggest that the most recent version of the UK’s physical climate model is
982 reproducing climate conditions consistent with the known changes to insolation during these two
983 warm periods, ~~and is consistent with previous versions of the same model, and other models.~~ Even
984 though the *lig127k* simulation did not contain any influx of Northern Hemisphere meltwater, shown
985 by previous work to be a critical forcing in LIG [simulations \(causing regions of both](#) warming [and](#)
986 [cooling, according to location\)](#), it is still nevertheless showing increased temperatures in certain
987 regions. ~~A potential caveat of this conclusion, however, is the matter of spin-up and the fact that~~
988 ~~neither of the current warm climate simulations were in oceanic equilibrium when the production runs~~
989 ~~were undertaken. The production runs were undertaken nevertheless because the resources required~~
990 ~~to run for several thousands of years (needed to reach true oceanic equilibrium) would have been~~
991 ~~impossible to obtain, but future simulations using this model should endeavour to obtain a better level~~
992 ~~of oceanic equilibrium.~~ Another limitation of using this particular version of the model is that certain
993 processes, such as vegetation and atmospheric chemistry, were prescribed, rather than allowed to be
994 dynamically evolving. Moreover, for ~~reasons of necessity~~ [practical reasons](#) some of the boundary
995 conditions were left as PI, such as vegetation, ~~surface like,~~ anthropogenic deforestation and aerosols; a
996 better simulation might be achieved if these were prescribed for the MH [and LIG](#). Processes and
997 boundary conditions such as these may be of critical importance regarding climate sensitivity during
998 the MH and the LIG, and therefore ongoing work is underway to repeat both of these experiments
999 using the most recent version of the UK’s Earth Systems model, UKESM1. Here, although the
1000 atmospheric core is HadGEM3, UKESM1 contains many other earth system components (e.g.
1001 dynamic vegetation), and therefore in theory should be able to better reproduce these paleoclimate
1002 states.

1003

1004 **DATA AVAILABILITY**

1005 The model simulations will be uploaded in the near future to the Earth System Grid Federation
1006 (ESGF) WCRP Coupled Model Intercomparison Project (Phase 6), [located at https://esgf-](https://esgf-node.llnl.gov/projects/cmip6/)
1007 [node.llnl.gov/projects/cmip6/](https://esgf-node.llnl.gov/projects/cmip6/), but are not yet publicly available. The simulations are, however,
1008 available [to the public](#) by directly contacting the lead author. For the MH reconstructions, the data
1009 can be found within the Supplementary Online Material of Bartlein *et al.* (2011), at
1010 <https://link.springer.com/article/10.1007/s00382-010-0904-1>. For the LIG [temperature](#)
1011 reconstructions, the data can be found within the Supplementary Online Material of Capron *et al.*
1012 (2017), at <https://www.sciencedirect.com/science/article/pii/S0277379117303487?via%3Dihub>, and
1013 the Supplementary Online Material of Hoffman *et al.* (2017), at
1014 <https://science.sciencemag.org/content/suppl/2017/01/23/355.6322.276.DC1>. [The LIG temperature](#)
1015 [reconstructions created here, based on the above Hoffman et al. \(2017\) data, are currently available by](#)
1016 [directly contacting the lead author. For the LIG precipitation reconstructions, the data can be found](#)
1017 [within the Supplementary Online Material of Scussolini et al. \(2019\), at](#)
1018 <https://advances.sciencemag.org/content/suppl/2019/11/18/5.11.eaax7047.DC1>.

1019

1020 **COMPETING INTERESTS**

1021 The authors declare that they have no conflict of interest.

1022

1023 **AUTHOR CONTRIBUTION**

1024 CJRW conducted the *midHolocene* simulation, carried out the analysis, produced the figures, wrote
1025 the majority of the manuscript, and led the paper. MVG conducted and provided the *lig127k*
1026 simulation, and contributed to some of the analysis and writing. EC provided the proxy data, and
1027 contributed to some of the writing. IMV provided the HadCM3 LIG simulation. PJV provided the
1028 HadCM3 MH simulation. JS contributed to some of the writing. All authors proofread the
1029 manuscript and provided comments.

1030

1031 **ACKNOWLEDGEMENTS**

1032 CJRW acknowledges the financial support of the UK Natural Environment Research Council-funded
1033 SWEET project (Super-Warm Early Eocene Temperatures), research grant NE/P01903X/1. CJRW
1034 also acknowledges the financial support of the Belmont-funded PACMEDY (PALaeo-Constraints on
1035 Monsoon Evolution and Dynamics) project, as does JS. MVG and LCS acknowledge the financial
1036 support of the NERC research grants NE/P013279/1 and NE/P009271/1. EC acknowledges financial
1037 support from the ChronoClimate project, funded by the Carlsberg Foundation.

1038 **REFERENCES**

- 1039 Bartlein, P. J., Harrison, S. P., Brewer, S., et al.: Pollen-based continental climate reconstructions at 6
1040 and 21 ka: a global synthesis, *Clim. Dyn.*, 37: 775–802, DOI:10.1007/s00382-010-0904-1, 2011
1041
- 1042 Berger, A. L.: Long-term variations of daily insolation and Quaternary climatic changes, *J. Atmos.*
1043 *Sci.*, 35: 2362-2367, [https://doi.org/10.1175/1520-0469\(1978\)035<2362:LTVODI>2.0.CO;2](https://doi.org/10.1175/1520-0469(1978)035<2362:LTVODI>2.0.CO;2), 1978
1044
- 1045 Berger, A. L. & Loutre, M. F.: Insolation values for the climate of the last 10,000,000 years,
1046 *Quaternary Sci. Rev.*, 10: 297–317, [https://doi.org/10.1016/0277-3791\(91\)90033-Q](https://doi.org/10.1016/0277-3791(91)90033-Q), 1991
1047
- 1048 Braconnot, P., Harrison, S. P., Kageyama, M., et al.: Evaluation of climate models using
1049 palaeoclimatic data, *nature Climate Change*, 2 (6): 417, DOI: 10.1038/NCLIMATE1456, 2012
1050
- 1051 Braconnot, P., Harrison, S. P., Otto-Bliesner, B, et al.: The palaeoclimate modelling intercomparison
1052 project contribution to CMIP5, *CLIVAR Exch. Newsl.*, 56: 15–19, 2011
1053
- 1054 Braconnot, P., Otto-Bliesner, B., Harrison, S., et al.: Results of PMIP2 coupled simulations of the
1055 Mid-Holocene and Last Glacial Maximum – Part 1: experiments and large-scale features, *Clim. Past*,
1056 3: 261-277, <https://doi.org/10.5194/cp-3-261-2007>, 2007
1057
- 1058 Brierley, C. M., Zhao, A., Harrison, S., et al.: Large-scale features and evaluation of the PMIP4-
1059 CMIP6 midHolocene simulations, *Clim. Past*, Under review
1060
- 1061 Capron, E., Govin, A., Stone, E. J., et al.: Temporal and spatial structure of multi-millennial
1062 temperature changes at high latitudes during the Last Interglacial, *Quat. Sci. Rev.*, 103: 116-133,
1063 <https://doi.org/10.1016/j.quascirev.2014.08.018>, 2014
1064
- 1065 Capron, E., Govin, A., Feng R. et al.: Critical evaluation of climate syntheses to benchmark
1066 CMIP6/PMIP4 127 ka Last Interglacial simulations in the high-latitude regions, *Quat. Sci. Rev.*, 168:
1067 137-150, DOI: 10.1016/j.quascirev.2017.04.019, 2017
1068
- 1069 Carlson, A. E.: Why there was not a Younger Dryas-like event during the Penultimate Deglaciation,
1070 *Quaternary Sci. Rev.*, 27: 882-887, DOI: 10.1016/j.quascirev.2008.02.004, 2008
1071
- 1072 Drake, N. A., Blench, R. M., Armitage, S. J., et al.: Ancient watercourses and biogeography of the
1073 Sahara explain the peopling of the desert, *proceedings of the National Academy of Sciences*, 108 (2):
1074 458-462, DOI: 10.1073/pnas.1012231108, 2011

1075
1076 Fischer, H., Meissner, K. J., Mix, A. C. et al.: Palaeoclimate constraints on the impact of 2°C
1077 anthropogenic warming and beyond, *nature Geoscience*, 11: 474-485, [https://doi.org/10.1038/s41561-](https://doi.org/10.1038/s41561-018-0146-0)
1078 018-0146-0, 2018
1079
1080 Gates, W. L.: The numerical simulation of ice-age climate with a global general circulation model, *J.*
1081 *Atmos. Sci*, 33: 1844–1873, DOI: 10.1175/1520-0469(1976)033<1844:TNSOIA>2.0.CO;2, 1976
1082
1083 Gregoire, L. J., Valdes, P. J., Payne, A. J. & Kahana, R.: Optimal tuning of a GCM using modern and
1084 glacial constraints, *Clim Dyn*, 37: 705-719, DOI:10.1007/s00382-010-0934-8, 2011
1085
1086 Guarino, M. V., Sime, L., Schroeder, D., et al.: Machine dependence and reproducibility for coupled
1087 climate simulations: The HadGEM3-GC3.1 CMIP Preindustrial simulation, *GMD*, 13 (1): 139-154,
1088 <https://doi.org/10.5194/gmd-2019-83>, 2020
1089
1090 Guarino, M. V. et al.: A sea ice-free Arctic during the Last Interglacial supports fast future loss,
1091 *Nature Climate Change*, Under review
1092
1093 Gunnar, M., Highwood, E. J., Shin, K. P. & Stordal, F.: New estimates of radiative forcing due to
1094 well mixed greenhouse gases, *Geophys. Res. Lett*, 25 (14): 2715-2718,
1095 <https://doi.org/10.1029/98GL01908>, 1998
1096
1097 Harrison, S. P., Bartlein, P. J., Brewer, S., et al.: Climate model benchmarking with glacial and mid-
1098 Holocene climates, *Clim. Dyn*, 43: 671–688, <https://doi.org/10.1007/s00382-013-1922-6>, 2014
1099
1100 Harrison, S. P., Bartlein, P. J., Izumi, K., et al.: Evaluation of CMIP5 palaeo-simulations to improve
1101 climate projections, *nature Climate Change*, 5: 735, DOI: 10.1038/nclimate2649, 2015
1102
1103 Haxeltine, A. & Prentice, I. C.: BIOME3: an equilibrium terrestrial biosphere model based on
1104 ecophysiological constraints, resource availability, and competition among plant functional types,
1105 *global Biogeochemical Cycles*, 10 (4): 693-709, DOI: 10.1029/96GB02344, 1996
1106
1107 Haywood, A. M., Dowsett, H. J., Dolan, A. M. et al.: The Pliocene Model Intercomparison Project
1108 (PlioMIP) Phase 2: scientific objectives and experimental design, *Clim. Past*, 12: 663-675,
1109 <https://doi.org/10.5194/cp-12-663-2016>, 2016
1110

1111 Haug, G., Hughen, K. A., Sigman, D. M., et al.: Southward migration of the intertropical convergence
1112 zone through the Holocene, *Science*, 293: 1304-1308, DOI: 10.1126/science.1059725, 2001
1113

1114 Hoelzmann, P., Jolly, D., Harrison, S. P., et al.: Mid-Holocene land-surface conditions in northern
1115 Africa and the Arabian Peninsula: A data set for the analysis of biogeophysical feedbacks in the
1116 climate system, *Global Biogeochemical Cycles*, 12 (1): 35-51, <https://doi.org/10.1029/97GB02733>,
1117 1998
1118

1119 Hoffman, J. S., Clark, P. U., Parnell, A. C., et al.: Regional and global sea-surface temperatures
1120 during the last interglaciation, *Science*, 355: 276-279, DOI: 10.1126/science.aai8464, 2017
1121

1122 Hollingsworth, A., Kållberg, P., Renner, V. & Burridge, D. M.: ‘An internal symmetric
1123 computational instability, *QJRM*, 109: 417–428, <https://doi.org/10.1002/qj.49710946012>, 1983
1124

1125 Holloway, M. D., Sime, L. C., Singarayer, J. S., et al.: Antarctic last interglacial isotope peak in
1126 response to sea ice retreat not ice-sheet collapse, *Nature Comms*, 7: 12293,
1127 <https://doi.org/10.1038/ncomms12293>, 2016
1128

1129 Jungclauss, J. H., Bard, E., Baroni, M. et al.: The PMIP4 contribution to CMIP6 – Part 3: The last
1130 millennium, scientific objective, and experimental design for the PMIP4 past1000 simulations, *GMD*,
1131 10: 4005-4033, <https://doi.org/10.5194/gmd-10-4005-2017>, 2017
1132

1133 Jolly, D., Harrison, S. P., Damnati, B. & Bonnefille, R.: Simulated climate and biomes of Africa
1134 during the Late Quaternary: Comparison with pollen and lake status data, *Quat. Sci. Rev.*, 17 (6-7):
1135 629-657, [https://doi.org/10.1016/S0277-3791\(98\)00015-8](https://doi.org/10.1016/S0277-3791(98)00015-8), 1998a
1136

1137 Jolly, D., Prentice, I. C., Bonnefille, R. et al.: Biome reconstruction from pollen and plant macrofossil
1138 data for Africa and the Arabian peninsula at 0 and 6000 years, *J. Biogeography*, 25 (6): 1007-1027,
1139 <https://www.jstor.org/stable/2846197>, 1998b
1140

1141 Joussaume, S. & Braconnot, P.: Sensitivity of paleoclimate simulation results to season definitions, *J.*
1142 *Geophys. Res.-Atmos*, 102: 1943-1956,
1143 <https://agupubs.onlinelibrary.wiley.com/doi/pdf/10.1029/96JD01989>, 1997
1144

1145 Joussaume, S. & Taylor K. E.: Status of the Paleoclimate Modeling Intercomparison Project,
1146 *Proceedings of the First International AMIP Scientific Conference*, WCRP-92 425, 430 Monterey,
1147 USA, 1995

1148
1149 Jousseaume, S., Taylor, K. E., Braconnot, P. et al.: Monsoon changes for 6000 years ago: Results of 18
1150 simulations from the Paleoclimate Modeling Intercomparison Project (PMIP), *GRL*, 26 (7): 859-862,
1151 <https://doi.org/10.1029/1999GL900126>, 1999
1152
1153 Kageyama, M., Albani, S., Braconnot, P. et al.: The PMIP4 contribution to CMIP6 – Part 4: Scientific
1154 objectives and experimental design of the PMIP4-CMIP6 Last Glacial Maximum experiments and
1155 PMIP4 sensitivity experiments, *GMD*, 10: 4035-4055, <https://doi.org/10.5194/gmd-10-4035-2017>,
1156 2017
1157
1158 Kageyama, M., Braconnot, P., Harrison, S. P. et al.: The PMIP4 contribution to CMIP6 – Part 1:
1159 Overview and over-arching analysis plan, *GMD*, 11: 1033-1057, [https://doi.org/10.5194/gmd-11-](https://doi.org/10.5194/gmd-11-1033-2018)
1160 [1033-2018](https://doi.org/10.5194/gmd-11-1033-2018), 2018
1161
1162 Kuhlbrodt, T., Jones, C. G., Sellar, A. et al.: The low resolution version of HadGEM3 GC3.1:
1163 Development and evaluation for global climate, *J. Adv. Model. Earth Sy*, 10: 2865-2888,
1164 <https://doi.org/10.1029/2018MS001370>, 2018
1165
1166 Kutzbach, J. E., Liu, X., Liu, Z. & Chen, G.: Simulation of the evolutionary response of global
1167 summer monsoons to orbital forcing over the past 280,000 years, *Clim. Dyn*, 30: 567-579, DOI:
1168 [10.1007/s00382-007-0308-z](https://doi.org/10.1007/s00382-007-0308-z), 2008
1169
1170 Kohfeld, K. E., Graham, R. M., de Boer, A. M. et al.: Southern Hemisphere westerly wind changes
1171 during the Last Glacial Maximum: paleo-data synthesis, *Quat. Sci. Rev*, 68: 76-95,
1172 <https://doi.org/10.1016/j.quascirev.2013.01.017>, 2013
1173
1174 Lézine, A. M., Hély, C., Grenier, C. et al.: Sahara and Sahel vulnerability to climate changes, lessons
1175 from Holocene hydrological data, *Quat. Sci. Rev*, 30 (21-22): 3001-3012,
1176 DOI:[10.1016/j.quascirev.2011.07.006](https://doi.org/10.1016/j.quascirev.2011.07.006), 2011
1177
1178 Liu, Z., Zhu, J., Rosenthal, Y. et al.: The Holocene temperature conundrum, *PNAS*, 111 (34): 3501-
1179 3505, DOI: [10.1073/pnas.1407229111](https://doi.org/10.1073/pnas.1407229111), 2014
1180
1181 Lunt, D. J., Abe-Ouchi, A., Bakker, P. et al.: A multi-model assessment of last interglacial
1182 temperatures, *Clim. Past*, 9: 699–717, <https://doi.org/10.5194/cp-9-699-2013>, 2013
1183

1184 Lunt, D. J., Foster, G. L., Haywood, A. M. & Stone, E. J.: Late Pliocene Greenland glaciation
1185 controlled by a decline in atmospheric CO₂ levels, *Nature*, 454 (7208): 1102, DOI:
1186 10.1038/nature07223, 2008
1187
1188 Marcott, S. A., Shakun, J. D., Clark, P. U. & Mix, A. C.: A reconstruction of regional and global
1189 temperature for the past 11,300 years, *Science*, 399 (6124): 1198-1201, DOI:
1190 10.1126/science.1228026, 2013
1191
1192 Marzocchi, A., Lunt, D. J., Flecker, R. et al.: Orbital control on late Miocene climate and the North
1193 African monsoon: insight from an ensemble of sub-precessional simulations, *Clim. Past*, 11 (10):
1194 1271-1295, <https://doi.org/10.5194/cp-11-1271-2015>, 2015
1195
1196 McGee, D., Donohoe, A., Marshall, J. & Ferreira, D.: Changes in ITCZ location and cross-equatorial
1197 heat transport at the Last Glacial Maximum, Heinrich Stadial 1, and the Mid-Holocene, *Earth and
1198 Planetary Science Letters*, 390: 69-79, <https://doi.org/10.1016/j.epsl.2013.12.043>, 2014
1199
1200 Menary, M. B., Kuhlbrodt, T., Ridley, J. et al.: Pre-industrial control simulations with HadGEM3-
1201 GC3.1 for CMIP6, *JAMES*, 10: 3049–3075, <https://doi.org/10.1029/2018MS001495>, 2018
1202
1203 New, M., Lister, D., Hulme, M. & Makin, I.: A high-resolution data set of surface climate over global
1204 land areas, *Clim Res*, 21: 2217–2238, DOI:10.3354/cr021001, 2002
1205
1206 Otto-Bliesner, B. L., Braconnot, P., Harrison, S. P. et al.: The PMIP4 contribution to CMIP6 – Part 2:
1207 Two interglacials, scientific objective and experimental design for Holocene and Last Interglacial
1208 simulations, *GMD*, 10: 3979-4003, <https://doi.org/10.5194/gmd-10-3979-2017>, 2017
1209
1210 Pollard, D. & Reusch, D. B.: A calendar conversion method for monthly mean paleoclimate model
1211 output with orbital forcing, *J. Geophys. Res*, 107 (D22), DOI:10.1029/2002JD002126, 2002
1212
1213 Rachmayani, R., Prange, M., Lunt, D. J., et al.: Sensitivity of the Greenland Ice Sheet to interglacial
1214 climate forcing: MIS 5e versus MIS11, *Paleoceanography*, 32 (11): 1089-1101,
1215 <https://doi.org/10.1002/2017PA003149>, 2017
1216
1217 Ramstein, G., Fluteau, F., Besse, J. & Joussaume, S.: Effect of orogeny, plate motion and land–sea
1218 distribution on Eurasian climate change over the past 30 million years, *Nature*, 386 (6627): 788,
1219 <https://doi.org/10.1038/386788a0>, 1997
1220

1221 Ridley, J., Blockley, E., Keen, A. B. et al.: The sea ice model component of HadGEM3-GC3.1, GMD,
1222 11: 713-723, <https://doi.org/10.5194/gmd-11-713-2018>, 2017
1223
1224 Rind, D. & Peteet, D.: Terrestrial conditions at the last glacial maximum and CLIMAP sea-surface
1225 temperature estimates: Are they consistent?, *Quat. Res.*, 2: 1-22, DOI:10.1016/0033-5894(85)90080-8,
1226 1985
1227
1228 Schmidt, G. A., Annan, J. D., Bartlein, P. J. et al.: Using paleo-climate comparisons to constrain
1229 future projections in CMIP5, *Clim. Past*, 10: 221-250, <https://doi.org/10.5194/cp-10-221-2014>, 2014
1230
1231 Scussolini, P., Bakker, P., Guo, C. et al.: Agreement between reconstructed and modeled boreal
1232 precipitation of the Last Interglacial, *Sci. Adv.*, 5 (11): 1-11,
1233 DOI: 10.1126/sciadv.aax7047, 2019
1234
1235 Singarayer, J. S. & Burrough, S. L.: Interhemispheric dynamics of the African rainbelt during the late
1236 Quaternary, *Quaternary Science Reviews*, 124: 48-67, DOI: 10.1016/j.quascirev.2015.06.021, 2015
1237
1238 Singarayer, J. S., Valdes, P. J. & Roberts, W. H. G.: Ocean dominated expansion and contraction of
1239 the late Quaternary tropical rainbelt, *Nature Scientific Reports*, 7: 9382, DOI:10.1038/s41598-017-
1240 09816-8, 2017
1241
1242 Smith, R. S. & Gregory, J. M.: A study of the sensitivity of ocean overturning circulation and climate
1243 to freshwater input in different regions of the North Atlantic, *Geophys. Res. Lett.*, 36,
1244 DOI:10.1029/2009GL038607, 2009
1245
1246 Stone, E. J., Capron, E., Lunt, D. J., et al.: Impact of meltwater on high-latitude early Last Interglacial
1247 climate, *Clim. Past*, 12: 1919–1932, <https://doi.org/10.5194/cp-12-1919-2016>, 2016
1248
1249 Storkey, D., Megann, A., Mathiot, P. et al.: UK Global Ocean GO6 and GO7: A traceable hierarchy
1250 of model resolutions, GMD, 11: 3187-3213, <https://doi.org/10.5194/gmd-11-3187-2018>, 2017
1251
1252 Taylor, K. E., Stouffer, R. J. & Meehl, G. A.: An overview of CMIP5 and the experiment design,
1253 *Bull. Am. Meteorol. Soc.*, 93: 485-498, <https://doi.org/10.1175/BAMS-D-11-00094.1>, 2011
1254
1255 Turney, C. S. M. & Jones, R. T.: Does the Agulhas Current amplify global temperatures during super-
1256 interglacials?, *J. Quat. Sci.*, 25 (6): 839-843, <https://doi.org/10.1002/jqs.1423>, 2010
1257

1258 Walters, D. N., A., Baran, I., Boutle, M. E. et al.: The Met Office Unified Model Global Atmosphere
1259 7.0/7.1 and JULES Global Land 7.0 configurations, *GMD*, 12: 1909-1923,
1260 <https://doi.org/10.5194/gmd-12-1909-2019>, 2017
1261
1262 Wang, X., et al.: Interhemispheric anti-phasing of rainfall during the last glacial period, *Quat. Sci.*
1263 *Rev*, 25: 3391-3403, DOI: 10.1016/j.quascirev.2006.02.009, 2006
1264
1265 Wang, Y., Cheng, H., Edwards, R.L., et al.: Millennial-and orbital-scale changes in the East Asian
1266 monsoon over the past 224,000 years, *Nature*, 451 (7182): 1090, DOI: 10.1038/nature06692, 2008
1267
1268 Wang, P. X., et al.: The global monsoon across timescales: coherent variability of regional monsoons,
1269 *Clim. Past*, 10: 2007-2052, <https://doi.org/10.5194/cp-10-2007-2014>, 2014
1270
1271 Williams, K. D., Copsey, D., Blockley E. W., et al.: The Met Office Global Coupled Model 3.0 and
1272 3.1 (GC3.0 and GC3.1) Configurations, *JAMES*, 10 (2): 357-380,
1273 <https://doi.org/10.1002/2017MS001115>, 2017
1274
1275

1276 **LIST OF TABLES**

1277 Table 1 - Astronomical parameters and atmospheric trace gas concentrations used in HadGEM3
1278 *midHolocene* and *lig127k* simulations

1279
1280 Table 2 - Trends (per century) in global mean measures of climate equilibrium for the last hundred
1281 years of the simulations, adapted from and including *piControl* results from Menary *et al.* (2018)

1282
1283 Table 3 - Global 1.5 m air temperature means and anomalies from HadGEM3 *piControl*,
1284 *midHolocene* and *lig127k* production runs (~~100-year climatology~~)

1285
1286 Table 4 - RMSE values (for various metrics) between simulations from different generations of the
1287 same model versus proxy data, and versus each other: a) MAT and MAP from the MH simulations
1288 versus proxy data from Bartlein *et al.* (2011); b) SST from the LIG simulations versus proxy data
1289 from Capron *et al.* (2017) and Hoffman *et al.* (2017). Regarding the proxy data comparisons in b), for
1290 JAS the simulated SST anomalies are compared to Northern Hemisphere summer reconstructions and
1291 for JFM the simulated SST anomalies are compared to Southern Hemisphere summer reconstructions

1292
1293 **LIST OF FIGURES**

1294 Figure 1 - Calendar adjusted Latitude~~latitude~~-month insolation (incoming SW radiative flux)
1295 anomalies: a) *midHolocene* - *piControl*; b) *lig127k* - *piControl*

1296
1297 ~~Fig_atmos_equilib~~ Annual global mean atmospheric fields from HadGEM3 *piControl*, *midHolocene*
1298 ~~and lig127k spin-up phases: a) 1.5 m air temperature; b) TOA. Thin lines in b) show annual TOA,~~
1299 ~~thick lines show 11-year running mean~~

1300
1301 ~~Fig_ocean_equilib~~ Annual global mean oceanic fields from HadGEM3 *piControl*, *midHolocene* and
1302 ~~lig127k spin-up phases: a) OeeTemp down to 1045m; b) OeeSal down to 1045m~~

1303
1304 Figure 2 – Calendar adjusted 1.5 m air temperature climatology differences, HadGEM3 *midHolocene*
1305 and *lig127k* production runs versus HadGEM3 *piControl* production run: a-c) *midHolocene* –
1306 *piControl*; d-f) *lig127k* – *piControl*. Top row: Annual; Middle row: Northern Hemisphere summer
1307 (JJA); Bottom row: Northern Hemisphere winter (DJF). Stippling shows statistical significance (as
1308 calculated by a Student’s T-test) at the 99% level

1309
1310 Figure 3 – Same as Figure 2, but for daily surface rainfall differences

1311

1312 [Figure 4 – Annual mean meridional overturning streamfunction climatologies from HadGEM3: a-c\)](#)
1313 [Atlantic basin; d-f\) Global. Top row: *piControl* simulation; Middle row: *midHolocene* simulation;](#)
1314 [Bottom row: *lig127k* simulation](#)

1315

1316 [Figure 5 – Calendar adjusted JJA daily surface rainfall & 850mb wind climatology differences,](#)
1317 [HadGEM3 *midHolocene* and *lig127k* production runs versus HadGEM3 *piControl* production run: a\)](#)
1318 [*midHolocene* – *piControl*; b\) *lig127k* – *piControl*; c\) *lig127k* – *midHolocene*](#)

1319

1320 [Figure 6 – Calendar adjusted JJA daily rainfall climatology by latitude, averaged over West Africa](#)
1321 [\(20°W-15°E, land points only\), for the various generations of the UK’s physical climate model: a\)](#)
1322 [Absolute values; b\) Anomalies \(MH or LIG – PI\). Solid lines show PI simulations, dashed lines show](#)
1323 [MH simulations and dotted lines show LIG simulations](#)

1324

1325 [Fig_latrain_prod – JJA rainfall differences by latitude, averaged over West Africa \(20°W-30°E,](#)
1326 [including both land and ocean points\), HadGEM3 *midHolocene* and *lig127k* production runs versus](#)
1327 [HadGEM3 *piControl* production run, 100-year climatology from each year](#)

1328

1329 [Fig_proxy_mh_loc – Simulated versus proxy MAT and MAP anomalies. Left hand side panels show](#)
1330 [simulated gridded anomalies from HadGEM3 \(*midHolocene* production run – *piControl* production](#)
1331 [run, 100-year climatology from each\), right hand side panels show proxy data from Bartlein *et al.*](#)
1332 [\(2011\) \(MH – preindustrial\). Proxy data locations are projected onto model grid: a\) Simulated MAT;](#)
1333 [b\) Proxy MAT; c\) Simulated MAP; d\) Proxy MAP](#)

1334

1335 [Figure 7 – Calendar adjusted mean annual surface air temperature anomalies from simulated model](#)
1336 [data versus proxy data. Background data show simulated anomalies \(MH – PI\) from different](#)
1337 [generations of the same model: a\) Proxy data anomalies \(MH – PI\) from Bartlein *et al.* \(2011\), with](#)
1338 [locations projected onto model grid; b\) HadGEM3; c\) HadGEM2-ES; d\) HadCM3](#)

1339

1340 [Figure 8 – Same as Figure 7, but for rainfall anomalies](#)

1341

1342 [Figure 9 – Calendar adjusted SST anomalies from model simulated data versus proxy data.](#)
1343 [Background data show simulated anomalies \(LIG - PI climatology\) from different generations of the](#)
1344 [same model, circles show proxy data anomalies \(LIG – preindustrial\) from Capron *et al.* \(2017\) and](#)
1345 [triangles show anomalies from Hoffman *et al.* \(2017\). Proxy data locations are projected onto model](#)
1346 [grid: a-c\) HadGEM3; d-f\) HadCM3. Top row: Annual; Middle row: Northern Hemisphere summer](#)
1347 [\(JAS\); Bottom row: Southern Hemisphere summer \(JFM\)](#)

1348
1349
1350
1351
1352
1353
1354
1355
1356
1357
1358
1359
1360
1361
1362
1363
1364
1365
1366
1367
1368
1369
1370
1371
1372
1373
1374

Figure 10 - Calendar adjusted annual surface rainfall anomalies from model simulated data versus proxy data. Background data show simulated anomalies (LIG - PI climatology) from different generations of the same model, circles show proxy data anomalies (LIG – preindustrial) from Scussolini et al. (2019). Proxy data locations are projected onto model grid: a) HadGEM3; b) HadCM3. Inset shows semi-quantitative scale of proxy data, adapted from Scussolini et al. (2019)

~~Fig_latrain_gen—JJA daily rainfall climatology differences (MH and LIG-PI) by latitude, averaged over West Africa (20°W–30°E, including both land and ocean points), for the various generations of the UK’s physical climate model, 100-year climatology from each (50-year climatology for HadCM3 LIG). Solid lines show MH simulations, dotted lines show LIG-simulations. Note that due to the low spatial resolution in HadCM3, values in-between latitude points have been interpolated~~

~~Fig_wafricarain_gen_mh—JJA daily rainfall climatology differences (MH-PI) for the various generations of the UK’s physical climate model, 100-year climatology from each: a) HadGEM3; b) HadGEM2-ES; c) HadCM3~~

~~Fig_wafricarain_gen_lig—JJA daily rainfall climatology differences (LIG-PI) for the various generations of the UK’s physical climate model, 100-year climatology from HadGEM3, 50-year climatology from HadCM3: a) HadGEM3; b) HadCM3~~

~~Fig_greening_prod—Annual mean rainfall over West Africa, zonally averaged from 20°W–30°E, HadGEM3 and CMIP5 midHolocene production run minus corresponding piControl production runs, 100-year climatology. Solid line shows HadGEM3, dotted lines show CMIP5 simulations. Grey dashes show maximum and minimum bounds of the increase in rainfall required to support grassland at each latitude, within which simulations must lie if producing enough rainfall to support grassland~~

1375 **LIST OF SUPPLEMENTARY MATERIAL FIGURES**

1376 SM1 – Latitude-month insolation (incoming SW radiative flux) anomalies, using modern
1377 calendar: a) *midHolocene - piControl*; b) *lig127k - piControl*

1378
1379 SM2 - Annual global mean atmospheric fields from HadGEM3 *piControl*, *midHolocene* and *lig127k*
1380 spin-up phases: a) 1.5 m air temperature; b) TOA radiation balance. Thin lines in b) show annual
1381 TOA radiation balance, thick lines show 11-year running mean. Note that the *piControl* spin-up
1382 phase was run in three separate parts, to accommodate for minor changes/updates in the model as the
1383 simulation progressed. Note also that the first ~50 years of the *lig127k* simulation have been
1384 deliberately removed from this figure, because a number of model crashes caused the model to be
1385 initially unstable and give highly varied global mean temperatures.

1386
1387 SM3 – Centennial trends in 1.5m temperature for HadGEM3 warm climate simulations' spin-up
1388 phases, last 100 years only: a) *midHolocene* ; b) *lig127k*. Stippling shows statistical significance (as
1389 calculated by a Mann-Kendall test) at the 99% level

1390
1391 SM4 - Annual global mean (full depth) oceanic fields from HadGEM3 *piControl*, *midHolocene* and
1392 *lig127k* spin-up phases: a) OceTemp; b) OceSal

1393
1394 SM5 – Modern calendar 1.5 m air temperature climatology differences, HadGEM3 *midHolocene* and
1395 *lig127k* production runs versus HadGEM3 *piControl* production run: a) *midHolocene - piControl*,
1396 JJA; b) *midHolocene - piControl*, DJF; c) *lig127k - piControl*, JJA; d) *lig127k - piControl*, DJF.
1397 Stippling shows statistical significance (as calculated by a Student's T-test) at the 99% level

1398
1399 SM6 – Annual mean sea-ice climatology differences, HadGEM3 *midHolocene* production run versus
1400 HadGEM3 *piControl* production run. Stippling shows statistical significance (as calculated by a
1401 Student's T-test) at the 99% level

1402 SM7 – Annual mean rainfall over West Africa (averaged over 20°W-30°E, consistent with Jousaume
1403 *et al.* [1999]), HadGEM3 *midHolocene* simulation minus corresponding *piControl*, and likewise for
1404 previous models from CMIP5. Solid line shows HadGEM3, dotted lines show CMIP5 simulations.
1405 Grey dashes show maximum and minimum bounds of the increase in rainfall required to support
1406 grassland at each latitude, within which simulations must lie if producing enough rainfall to support
1407 grassland (adapted from Figure 3a in Jousaume *et al.* [1999])

1410 TABLES

	<i>piControl</i>	<i>midHolocene</i>	<i>lig127k</i>
Astronomical parameters			
Eccentricity	0.016764	0.018682	0.039378
Obliquity	23.459	24.105°	24.04°
Perihelion-180°	100.33	0.87°	275.41°
Date of vernal equinox	March 21 at noon	March 21 at noon	March 21 at noon
Trace gases			
CO₂	284.3 ppm	264.4 ppm	275 ppm
CH₄	808.2 ppb	597 ppb	685 ppb
N₂O	273 ppb	262 ppb	255 ppb
Other GHG gases	CMIP DECK <i>piControl</i>	CMIP DECK <i>piControl</i>	CMIP DECK <i>piControl</i>

1411

1412 Table 1 - Astronomical parameters and atmospheric trace gas concentrations used in HadGEM3
1413 simulations

1414

1415

1416

Variable	<i>piControl</i>	<i>midHolocene</i>	<i>lig127k</i>
TOA (W m²)	-0.002	-0.05	-0.06
1.5 m air temp (°C)	0.03	-0.06	-0.16
OceTemp (°C)	0.035	0.03	0.03
OceSal (psu)	0.0001	-0.0004	0.00007

1417

1418 Table 2 - Trends (per century) in global mean measures of climate equilibrium for the last hundred
1419 years of the simulations, adapted from and including *piControl* results from Menary *et al.* (2018)

1420

1421

Time period	Means (°C)			Anomalies (°C)	
	<i>piControl</i>	<i>midHolocene</i>	<i>lig127k</i>	<i>midHolocene – piControl</i>	<i>lig127k – piControl</i>
Annual	13.8	13.67	14.29	-0.12	0.49
JJA	15.68	15.75	17.37	0.07	1.69
DJF	11.86	11.55	11.39	-0.31	-0.47

1422

1423 Table 3 - Global 1.5 m air temperature means and anomalies from HadGEM3 *piControl*,
1424 *midHolocene* and *lig127k* production runs

1425

1426

1427

1428

1429

1430

1431

1432

1433

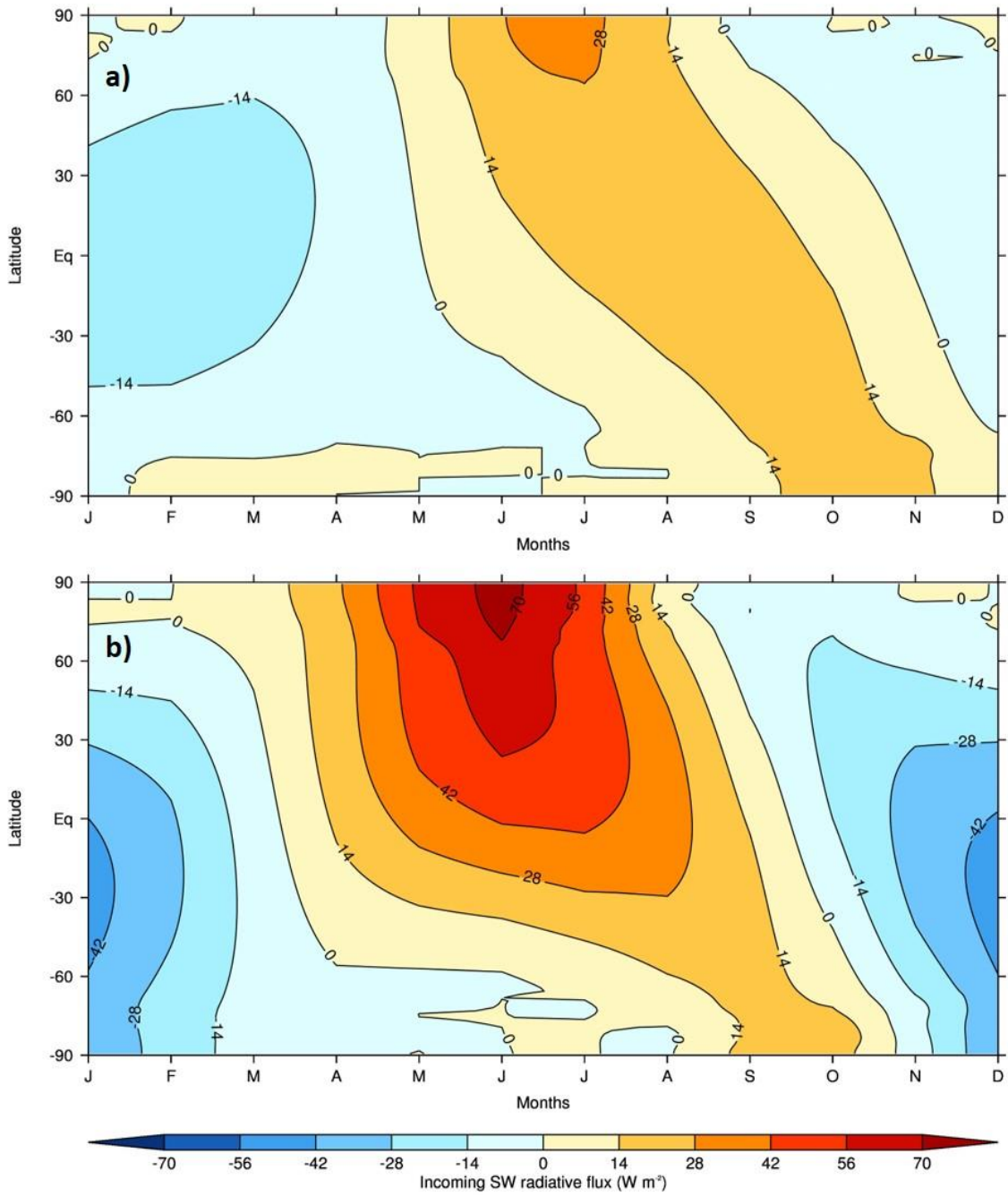
1434 a)
1435

Metric	Simulations vs proxy data			Simulations vs simulations	
	HadGEM3	HadGEM2-ES	HadCM3	HadGEM2-ES v HadGEM3	HadCM3 v HadGEM3
MAT (°C)	2.45	2.42	2.37	0.65	0.57
<i>No. of locations</i>	638			Global coverage	
MAP (mm year⁻¹)	285.9	293.5	304.7	90.8	121.8
<i>No. of locations</i>	651			Global coverage	

1436 b)
1437
1438

Metric	Simulations vs proxy data					
	Yearly		JAS		JFM	
	HadGEM3	HadCM3	HadGEM3	HadCM3	HadGEM3	HadCM3
SST from Capron <i>et al.</i> (2017)	3.03	3.04	3.03	2.98	2.81	2.62
<i>No. of locations</i>	3		24		15	
SST from Hoffman <i>et al.</i> (2017)	2.42	3.02	1.99	2.78	4.28	3.97
<i>No. of locations</i>	86		12		6	

1439 Table 4 - RMSE values (for various metrics) between simulations from different generations of the
1440 same model versus proxy data, and versus each other: a) MAT and MAP from the MH simulations
1441 versus proxy data from Bartlein *et al.* (2011); b) SST from the LIG simulations versus proxy data
1442 from Capron *et al.* (2017) and Hoffman *et al.* (2017). Regarding the proxy data comparisons in b), for
1443 JAS the simulated SST anomalies are compared to Northern Hemisphere summer reconstructions and
1444 for JFM the simulated SST anomalies are compared to Southern Hemisphere summer reconstructions
1445
1446
1447
1448

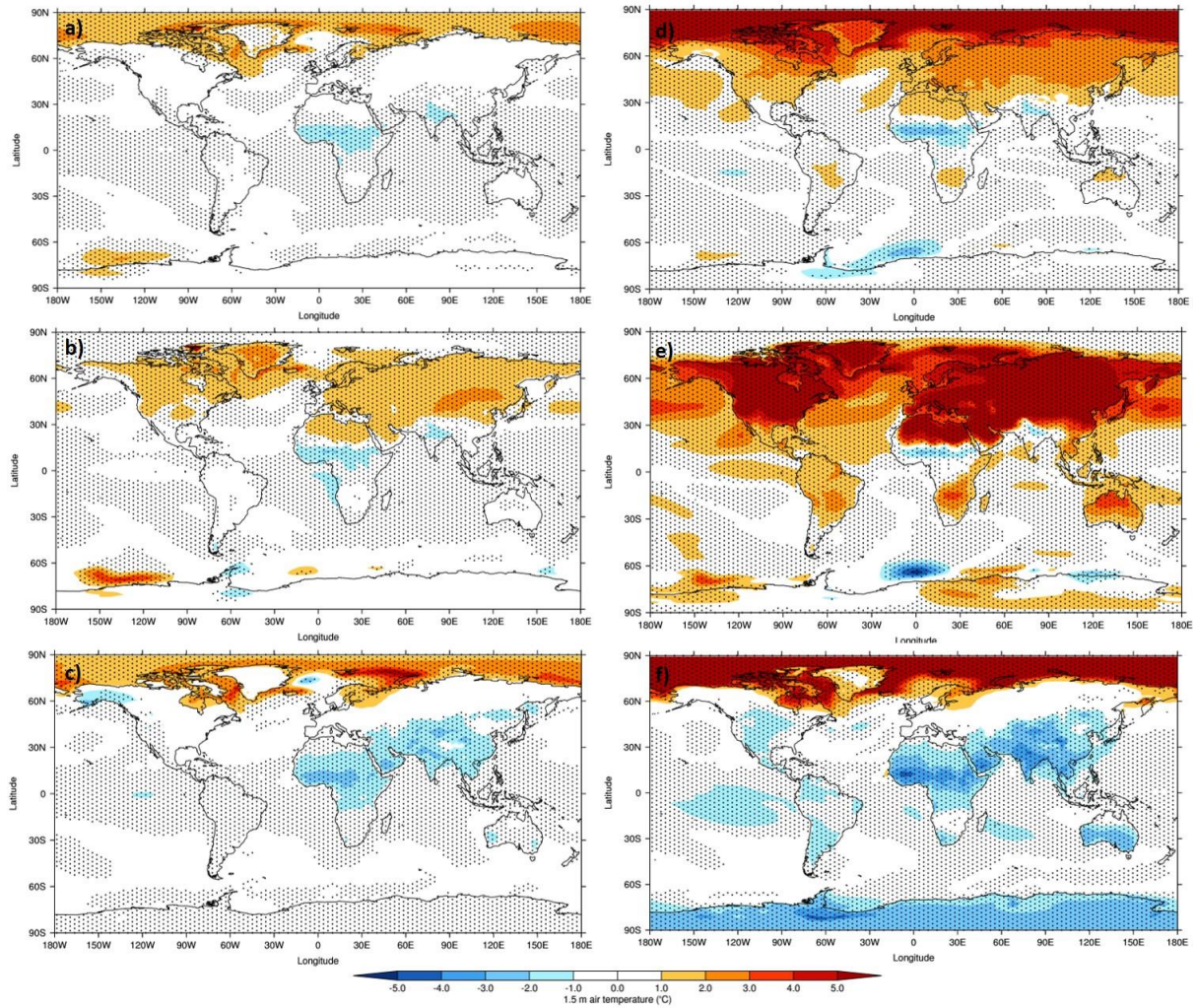


1450

1451 Figure 1 - Calendar adjusted Latitude-month insolation (incoming SW radiative flux)

1452 anomalies: a) *midHolocene - piControl*; b) *lig127k - piControl*

1453



1454

1455 Figure 2 – [Calendar adjusted](#) 1.5 m air temperature climatology differences, HadGEM3 *midHolocene*

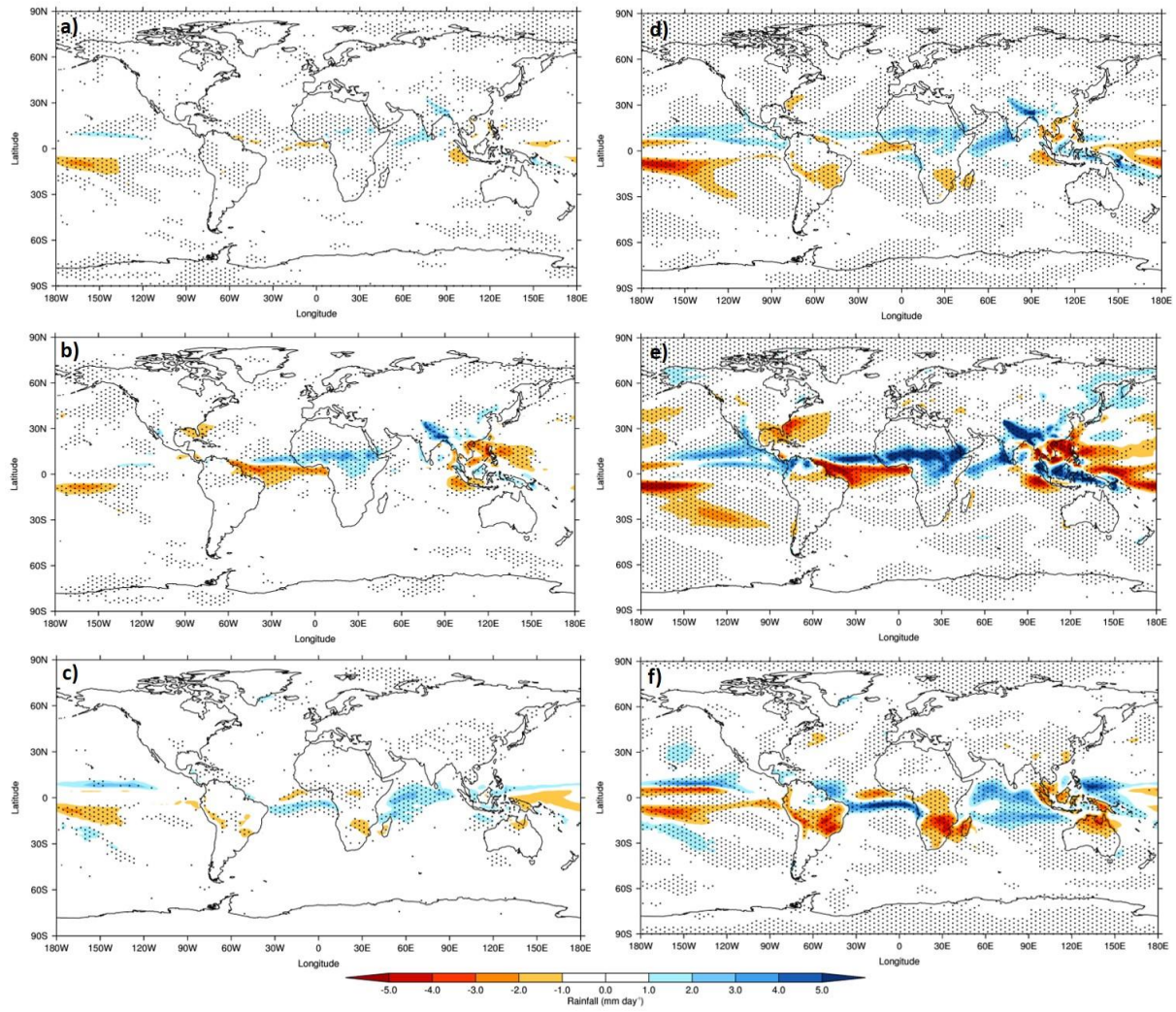
1456 and *lig127k* production runs versus HadGEM3 *piControl* production run: [a-c\) *midHolocene* –](#)

1457 [piControl](#); [d-f\) *lig127k* – piControl](#). Top row: Annual; Middle row: Northern Hemisphere summer

1458 [\(JJA\)](#); Bottom row: Northern Hemisphere winter (DJF). Stippling shows statistical significance (as

1459 [calculated by a Student’s T-test\) at the 99% level](#)

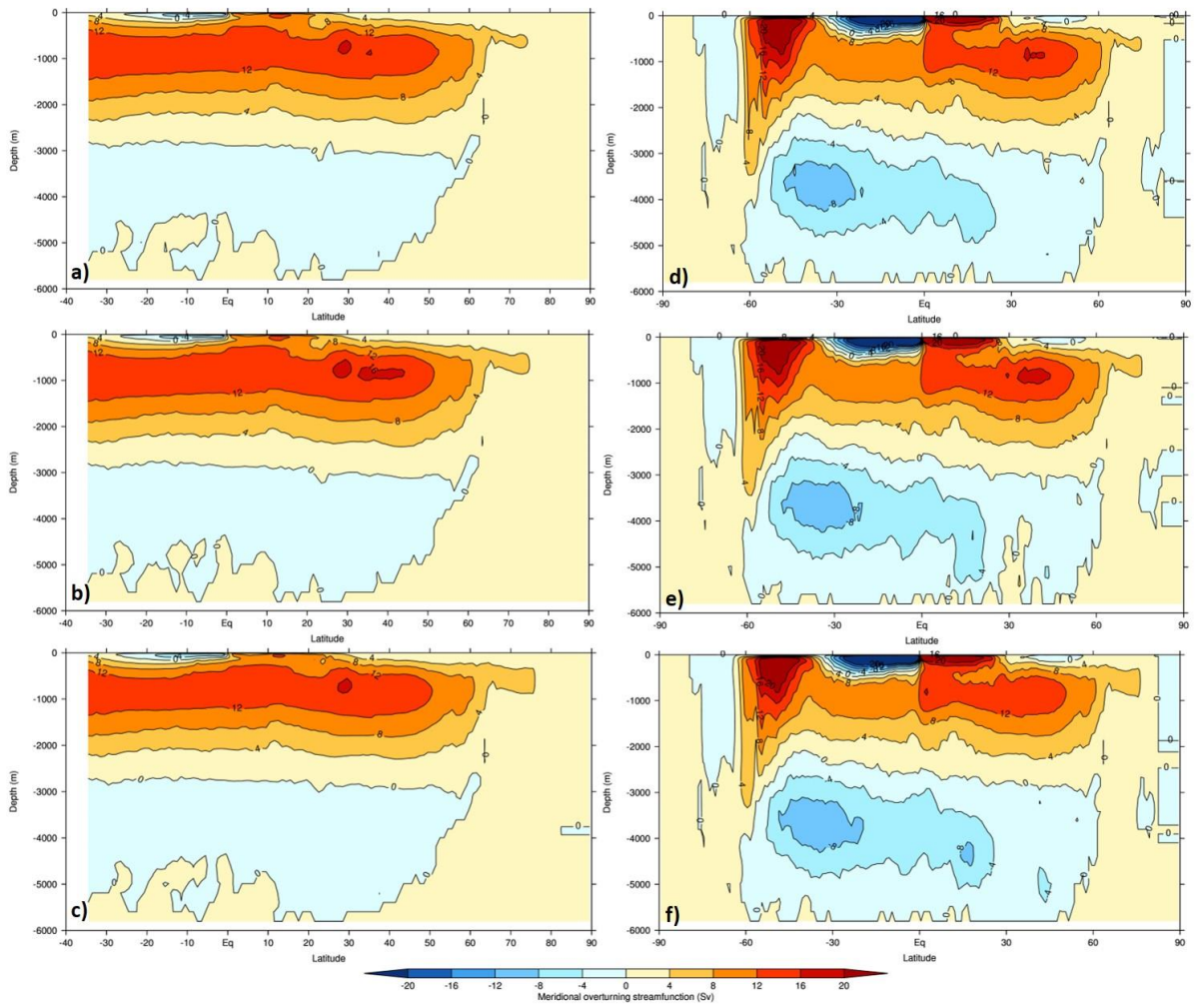
1460



1461

1462

Figure 3 – Same as Figure 2, but for daily surface rainfall differences



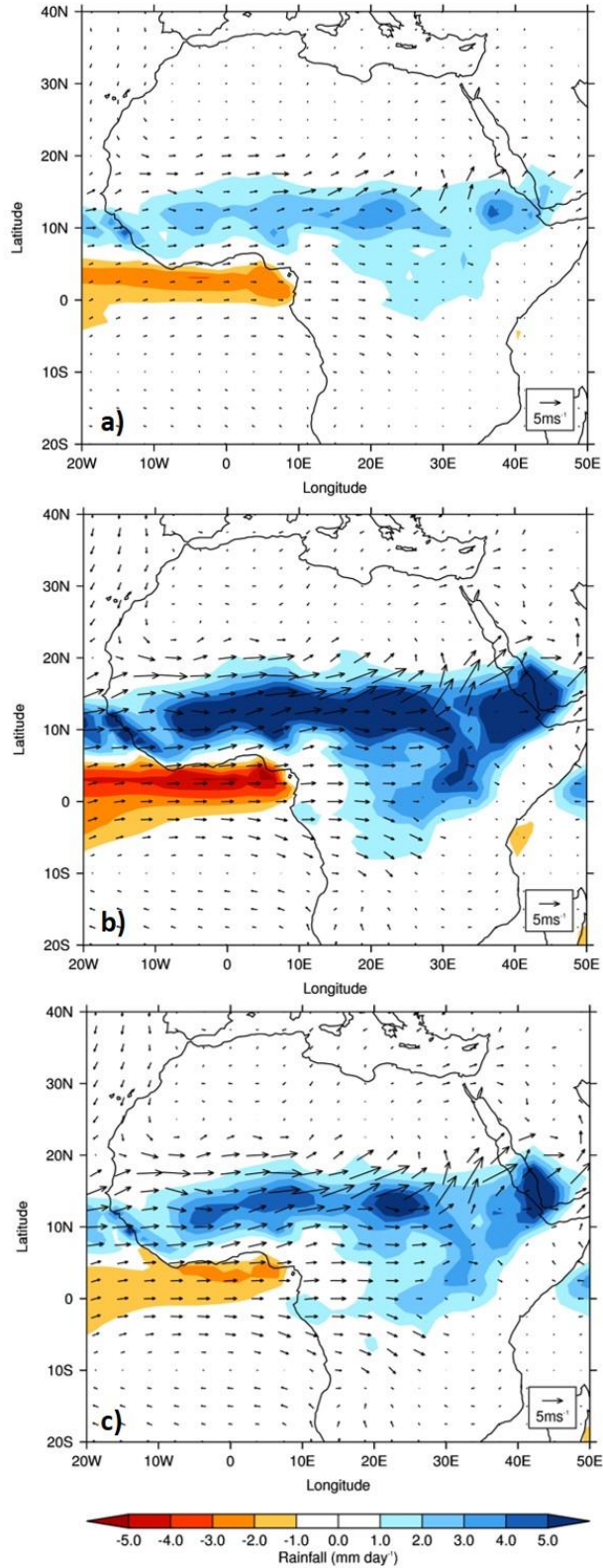
1463

1464 Figure 4 – Annual mean meridional overturning streamfunction climatologies from HadGEM3: a-c)

1465 Atlantic basin; d-f) Global. Top row: *piControl* simulation; Middle row: *midHolocene* simulation;

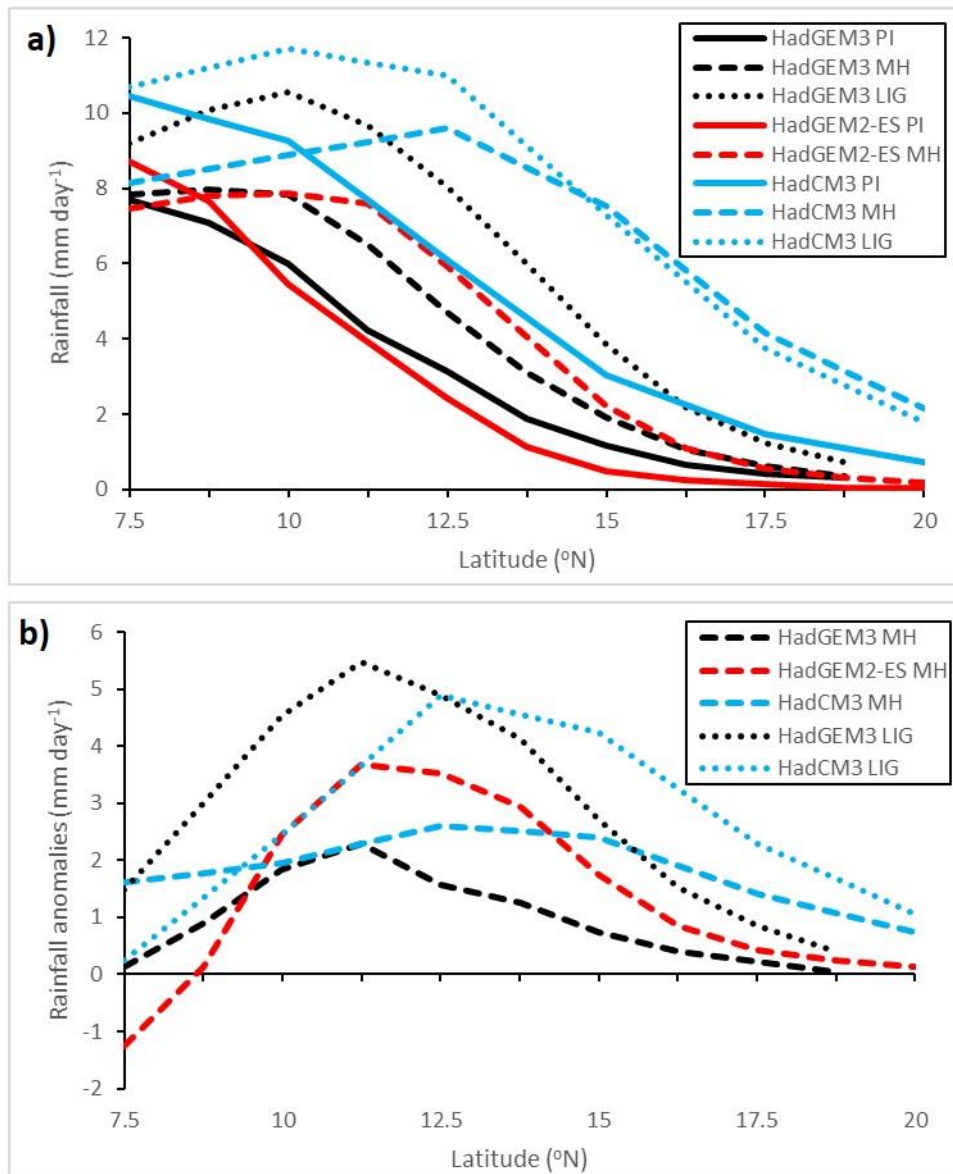
1466 Bottom row: *lig127k* simulation

1467



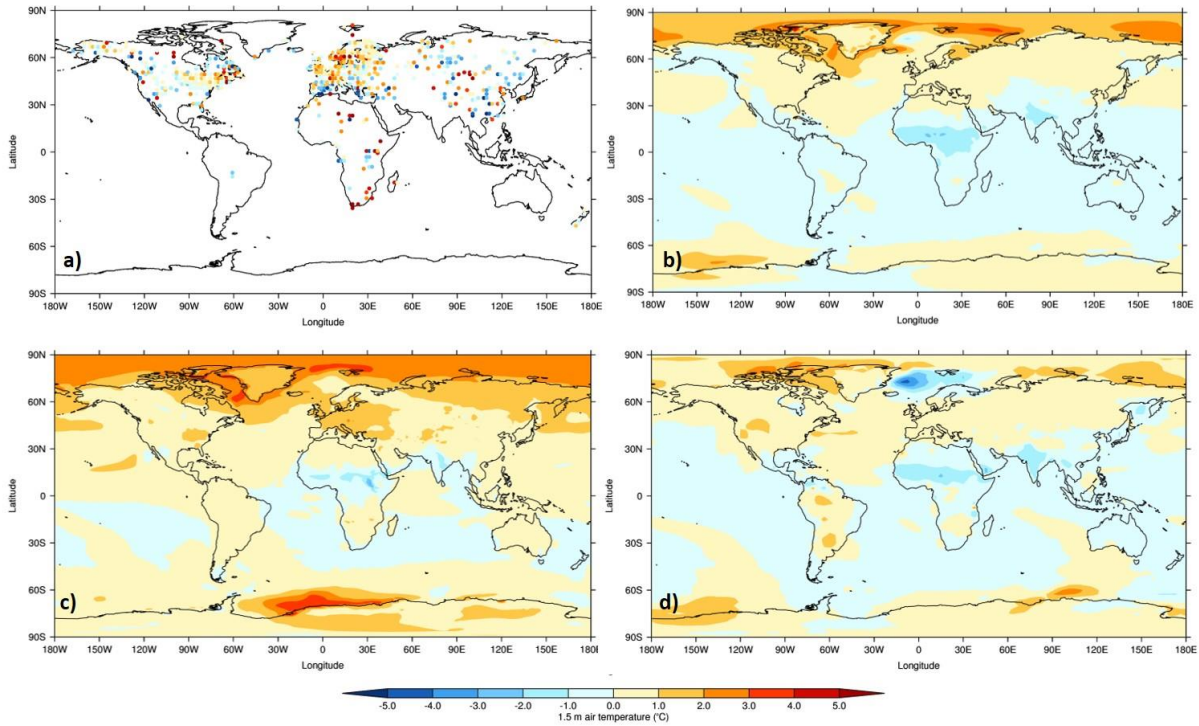
1468

1469 Figure 5 – Calendar adjusted JJA daily surface rainfall & 850mb wind climatology differences,
 1470 HadGEM3 *midHolocene* and *lig127k* production runs versus HadGEM3 *piControl* production run: a)
 1471 *midHolocene - piControl*; b) *lig127k - piControl*; c) *lig127k - midHolocene*



1472

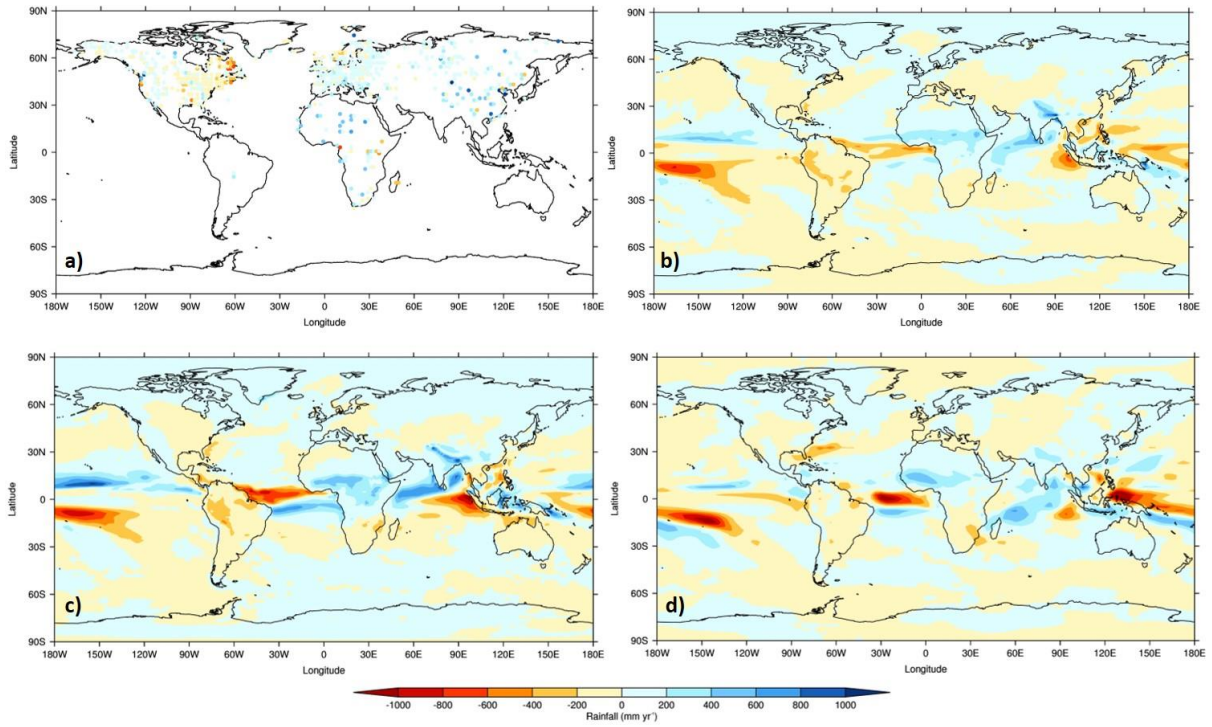
1473 Figure 6 – Calendar adjusted JJA daily rainfall climatology by latitude, averaged over West Africa
 1474 (20°W-15°E, land points only), for the various generations of the UK’s physical climate model: a)
 1475 Absolute values; b) Anomalies (MH or LIG – PI). Solid lines show PI simulations, dashed lines show
 1476 MH simulations and dotted lines show LIG simulations



1477

1478 Figure 7 – Calendar adjusted Mean-mean annual surface air temperature anomalies from simulated
 1479 model data versus proxy data versus calendar adjusted simulated anomalies. Background gridded
 1480 data show simulated anomalies (MH – PI) from different generations of the same model: a) Proxy
 1481 data anomalies (MH – PI) from Bartlein et al. (2011), with locations projected onto HadGEM3- model
 1482 grid; b) HadGEM3; c) HadGEM2-ES; d) HadCM3

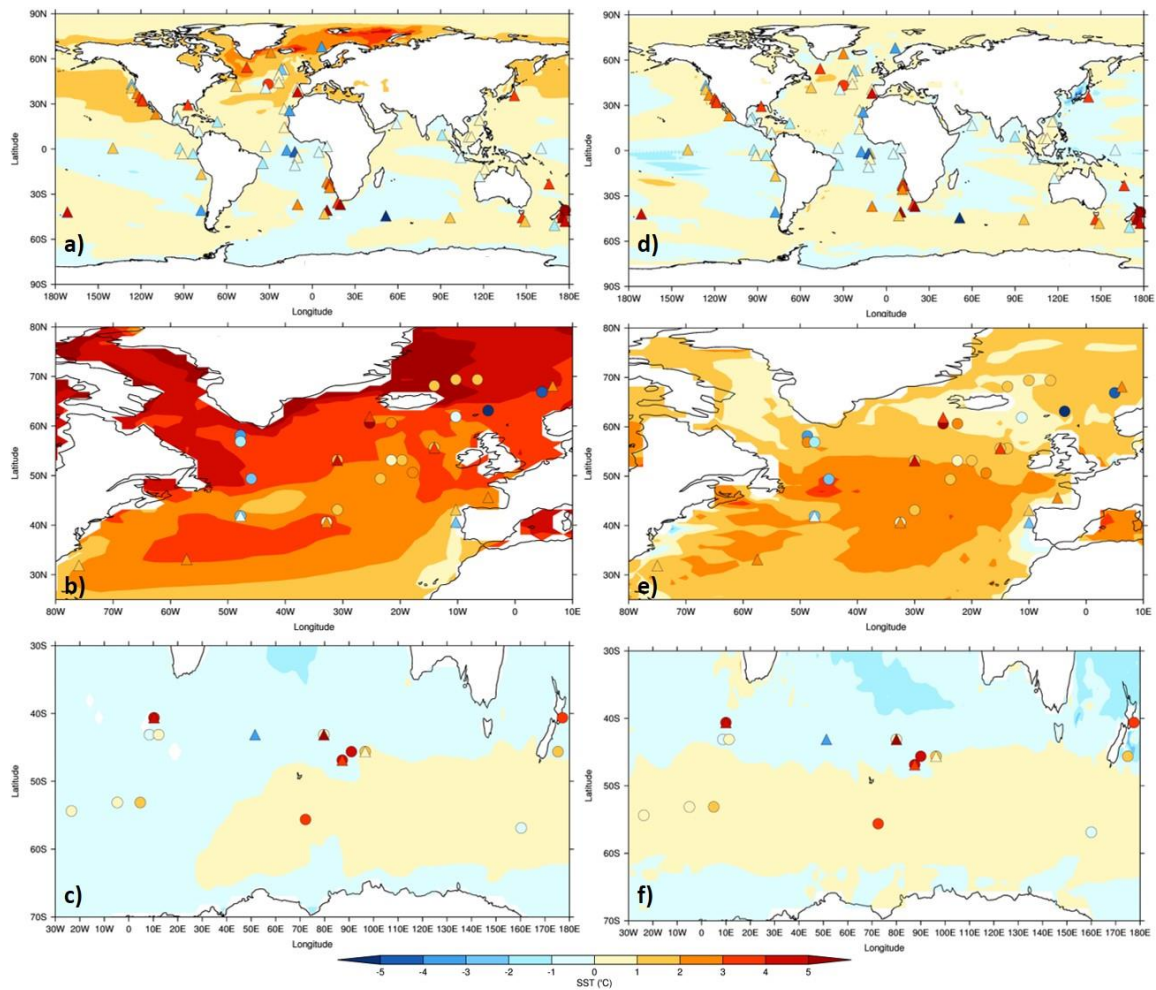
1483



1484

1485 Figure 8 – Same as Figure 7, but for rainfall anomalies

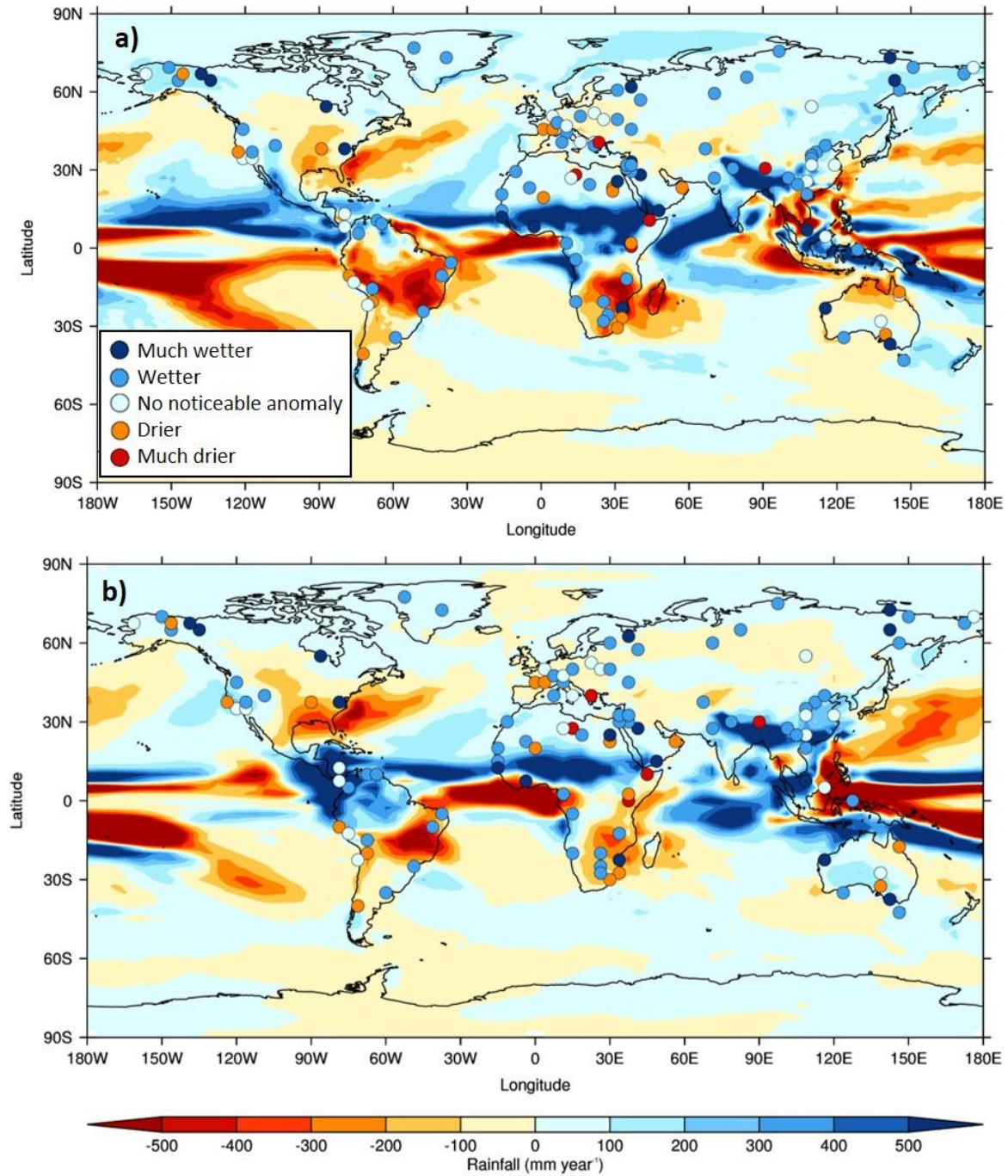
1486



1487

1488 Figure 9 - Calendar adjusted SST anomalies from model simulated data versus proxy data.

1489 Background gridded data show simulated anomalies (LIG - PI climatology) from different generations
 1490 of the same model, circles show proxy data anomalies (LIG – preindustrial) from Capron et al. (2017)
 1491 and triangles show anomalies from Hoffman et al. (2017). Proxy data locations are projected onto
 1492 model grid: a-c) HadGEM3; d-f) HadCM3. Top row: Annual; Middle row: Northern Hemisphere
 1493 summer (JAS); Bottom row: Southern Hemisphere summer (JFM)



1494

1495 Figure 10 - Calendar adjusted annual surface rainfall anomalies from model simulated data versus
 1496 proxy data. Background gridded data show simulated anomalies (LIG - PI climatology) from
 1497 different generations of the same model, circles show proxy data anomalies (LIG – preindustrial) from
 1498 Scussolini et al. (2019). Proxy data locations are projected onto model grid: a) HadGEM3; b)
 1499 HadCM3. Inset shows semi-quantitative scale of proxy data, adapted from Scussolini et al. (2019)
 1500

1
2
3
4
5
6
7
8
9
10
11
12
13
14
15
16
17
18

**CMIP6/PMIP4 simulations of the mid-Holocene and Last Interglacial using
HadGEM3: comparison to the pre-industrial era, previous model versions,
and proxy data**

**Charles J. R. Williams^{1,5}, Maria-Vittoria Guarino², Emilie Capron³, Irene Malmierca-
Vallet^{1,2}, Joy S. Singarayer^{4,1}, Louise C. Sime², Daniel J. Lunt¹, Paul J. Valdes¹**

¹School of Geographical Sciences, University of Bristol, UK (c.j.r.williams@bristol.ac.uk)

²British Antarctic Survey, Cambridge, UK

³Physics of Ice, Climate and Earth, Niels Bohr Institute, University of Copenhagen, Denmark

⁴Department of Meteorology & School of Archaeology, Geography and Environmental
Science, University of Reading, UK

⁵NCAS-Climate / Department of Meteorology, University of Reading, UK

SUPPLEMENTARY MATERIAL

19 **TEXT**

20 **Model description**

21 ~~However~~Here, a ~~brief~~ description of the major changes in the latest version of UK's physical climate
22 model, HadGEM3-GC3.1-GC3.1, relative to its predecessor, ~~are~~ is given, following on directly from
23 Section 2.1.2 in the main manuscript in the here. Beginning with Global Atmosphere (GA7) and
24 Global Land components (GL7), a once-in-a-decade replacement of the model's dynamical core,
25 implementing ENDGame, was undertaken for the previous version (GA6) and therefore remains the
26 same in GA7 (Walters *et al.* 2017)¹. A number of other developments, since the previous version of
27 the model, have also been included. In addition, a number of bottom-up and top-down developments
28 were included in GA7. For the former, these include improvementsImprovements were made to the
29 radiation scheme to allow better treatment of gases absorption, as well as improvements to how warm
30 rain and ice clouds are treated, ~~and~~ an improvement to the numerics of the convection scheme, and
31 ~~(Walters et al. 2017). For the latter, these include further~~ improvements to the microphysics as well
32 as an incremental development of ENDGame (Walters *et al.* 2017). Together these led to reductions
33 in four model errors that were deemed critical in the previous configuration: i) South Asian monsoon
34 rainfall biases over India; ii) biases in both temperature and humidity in the tropical tropopause; iii)
35 shortcomings in the numerical conservation; and iv) biases in surface radiation fluxes over the
36 Southern Ocean (Walters *et al.* 2017). In addition to these developments, two new parameterisation
37 schemes were introduced in GA7: firstly the UK Chemistry and Aerosol (UKCA) GLOMAP-mode
38 aerosol scheme, to improve the representation of tropospheric aerosols, and secondly a multi-layer
39 snow scheme in the Joint UK Land Environment Simulator (JULES)-JULES, to allow the first time
40 inclusion of stochastic physics in UM climate simulations (Walters *et al.* 2017).

41

42 For the Global Ocean (GO) and Global Sea Ice (GIS) components, a number of improvements to
43 GO6 have been made since the previous version, the first of which was an upgrade of the NEMO base
44 code (to version 3.6) which allowed a formulation for momentum advection (from Hollingsworth *et*
45 *al.* 1983), a Lagrangian icebergs scheme, and a simulation of circulation below ice shelves (Storkey *et*
46 *al.* 2018). Other developments included an improvement to the warm SST bias in the Southern Ocean
47 (as detailed by Williams *et al.* 2017), as well as tuning of various parameters e.g. the isopycnal
48 diffusion (Storkey *et al.* 2018). For GIS8, along with improvements to the albedo scheme and more
49 realistic semi-implicit coupling, the biggest development since its predecessor is the inclusion of
50 multilayer thermodynamics, giving a heat capacity to the sea ice and allowing vertical variation of
51 conduction (Ridley *et al.* 2018). Testing of these two components produced a better simulation
52 compared to its predecessor, with more realistic mixed layer depths in the Southern Ocean and the

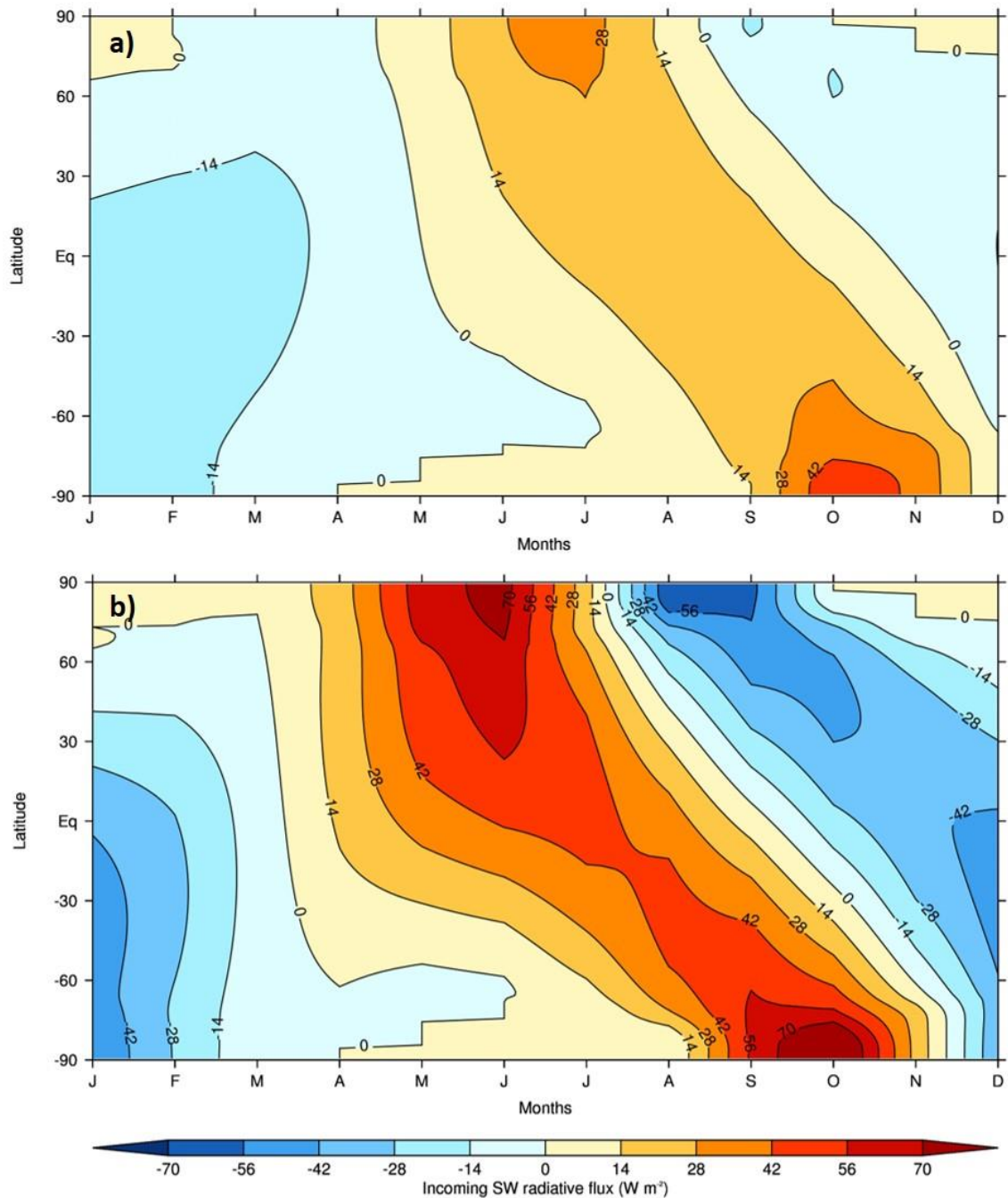
¹ Please see Reference section in main manuscript for citations

53 aforementioned reduced warm bias, the latter of which was deemed primarily due to the tuning of the
54 different mixing (e.g. vertical and isopycnal) parameters (Storkey *et al.* 2018).

55

56

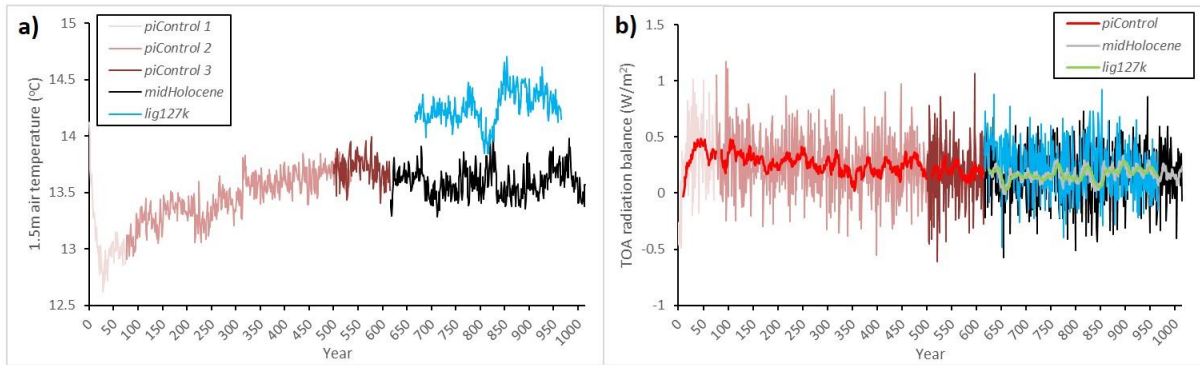
57 **FIGURES**



58

59 SM1 - Latitude-month insolation (incoming SW radiative flux) anomalies, using modern
60 calendar: a) *midHolocene - piControl*; b) *lig127k - piControl*

61



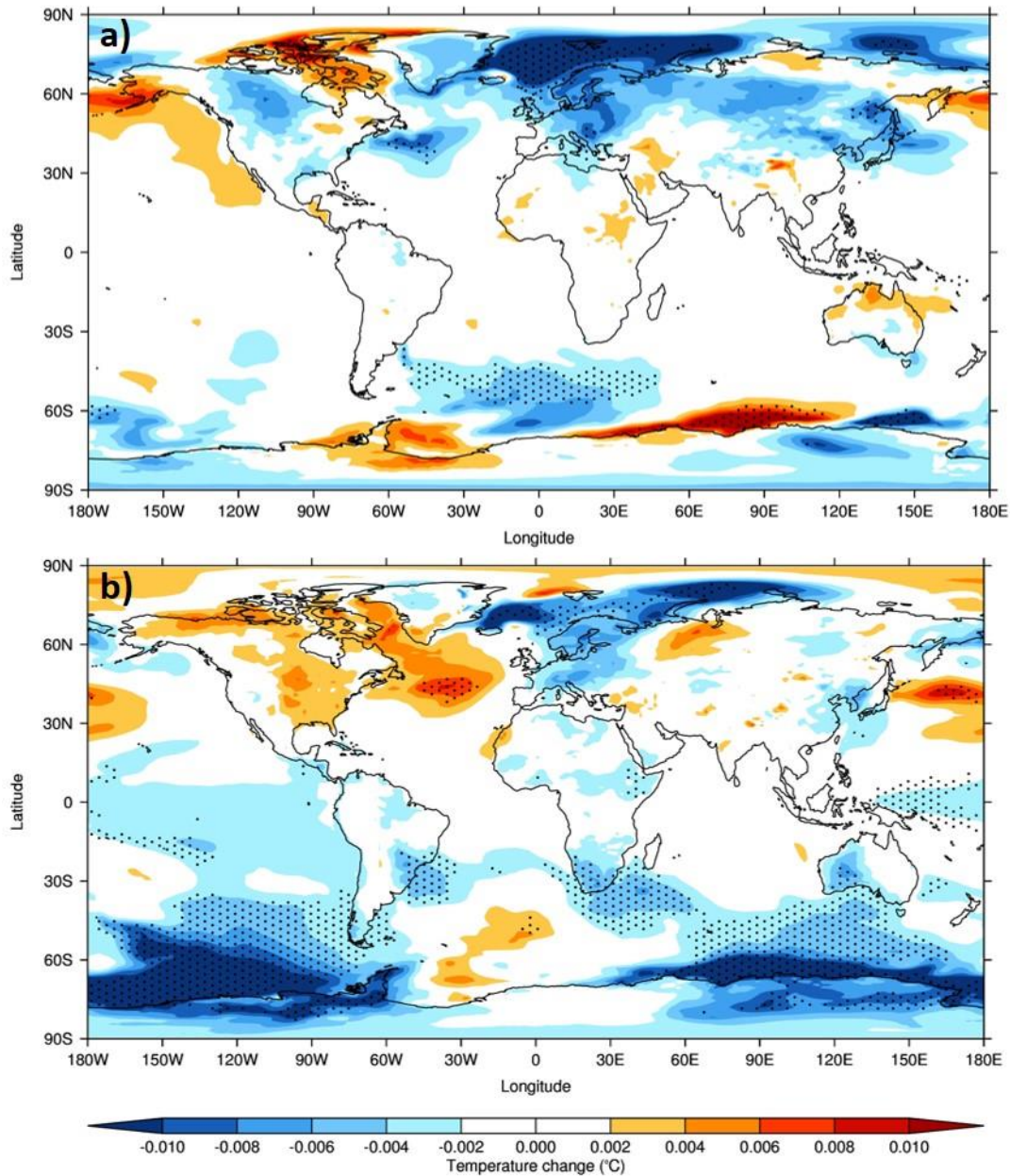
62

63 SM2 - Annual global mean atmospheric fields from HadGEM3 *piControl*, *midHolocene* and *lig127k*
 64 spin-up phases: a) 1.5 m air temperature; b) TOA radiation balance. Thin lines in b) show annual
 65 TOA radiation balance, thick lines show 11-year running mean. Note that the *piControl* spin-up
 66 phase was run in three separate parts, to accommodate for minor changes/updates in the model as the
 67 simulation progressed. Note also that the first ~50 years of the *lig127k* simulation have been
 68 deliberately removed from this figure, because a number of model crashes caused the model to be
 69 initially unstable and give highly varied global mean temperatures.

70

71

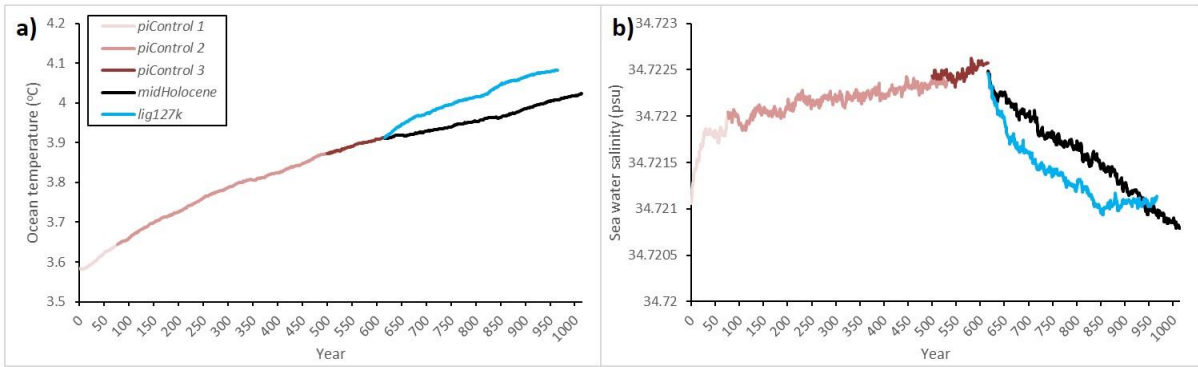
72



73

74 SM3 - Centennial trends in 1.5m temperature for HadGEM3 warm climate simulations' spin-up
 75 phases, last 100 years only: a) *midHolocene* ; b) *lig127k*. Stippling shows statistical significance (as
 76 calculated by a Mann-Kendall test) at the 99% level

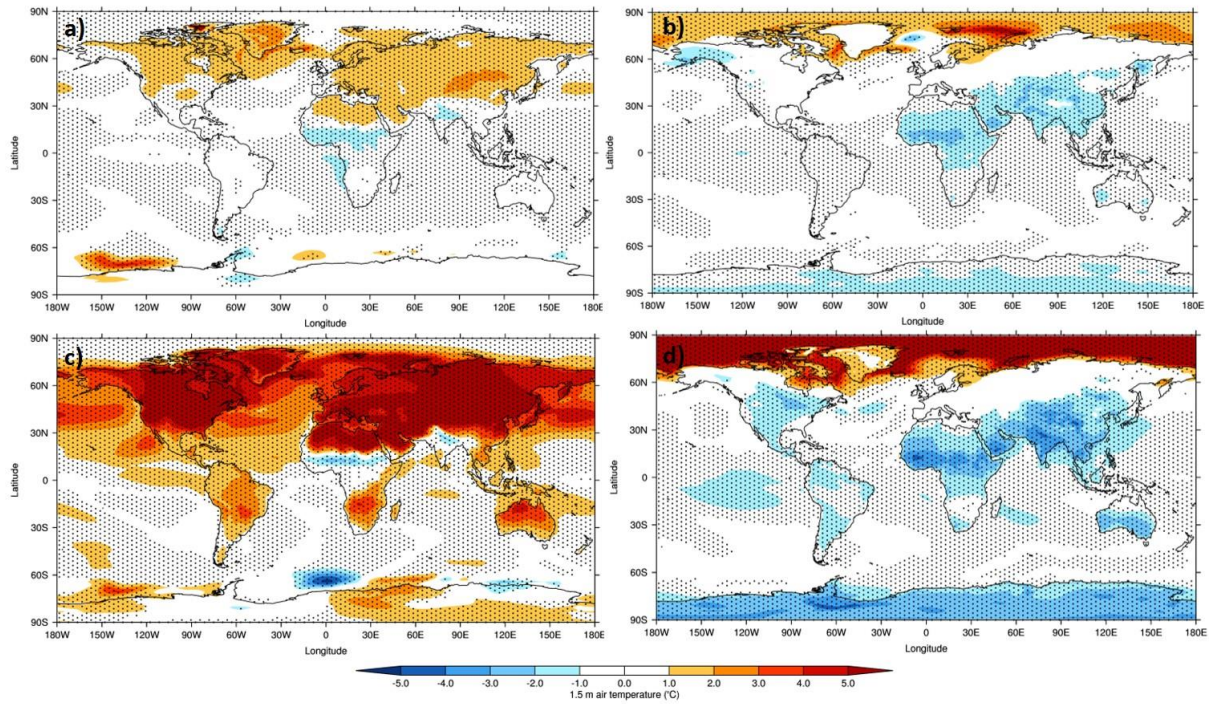
77



78

79 SM4 - Annual global mean (full depth) oceanic fields from HadGEM3 *piControl*, *midHolocene* and
 80 *lig127k* spin-up phases: a) OceTemp; b) OceSal

81



82

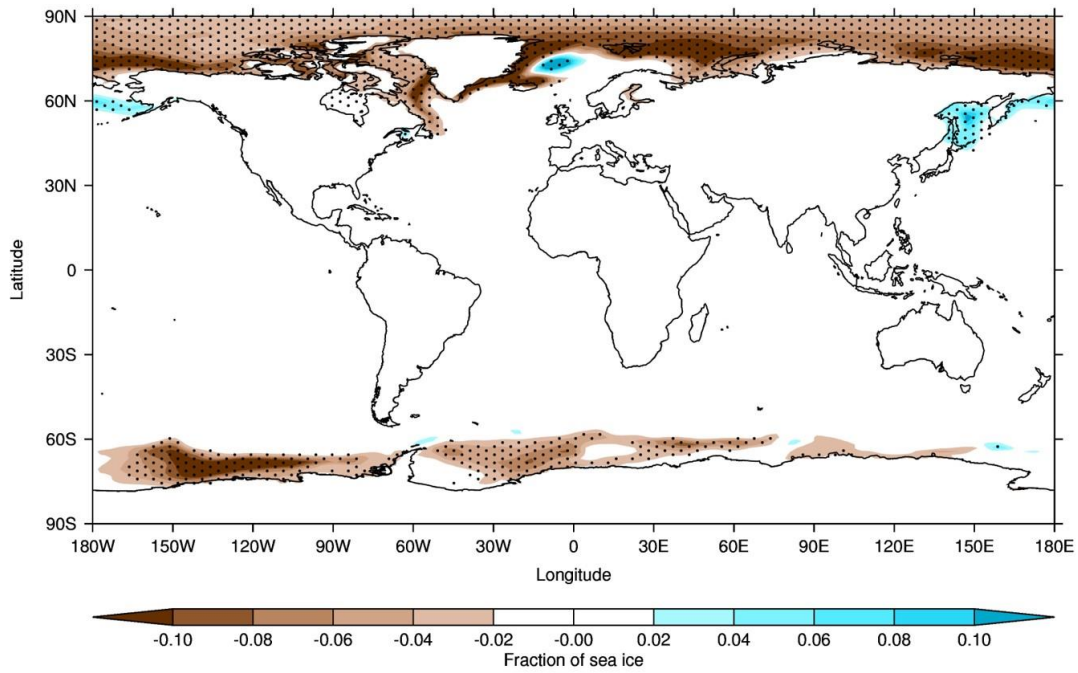
83 SM5 - Modern calendar 1.5 m air temperature climatology differences, HadGEM3 *midHolocene* and

84 *lig127k* production runs versus HadGEM3 *piControl* production run: a) *midHolocene* - *piControl*,

85 JJA; b) *midHolocene* - *piControl*, DJF; c) *lig127k* - *piControl*, JJA; d) *lig127k* - *piControl*, DJF.

86 Stippling shows statistical significance (as calculated by a Student's T-test) at the 99% level

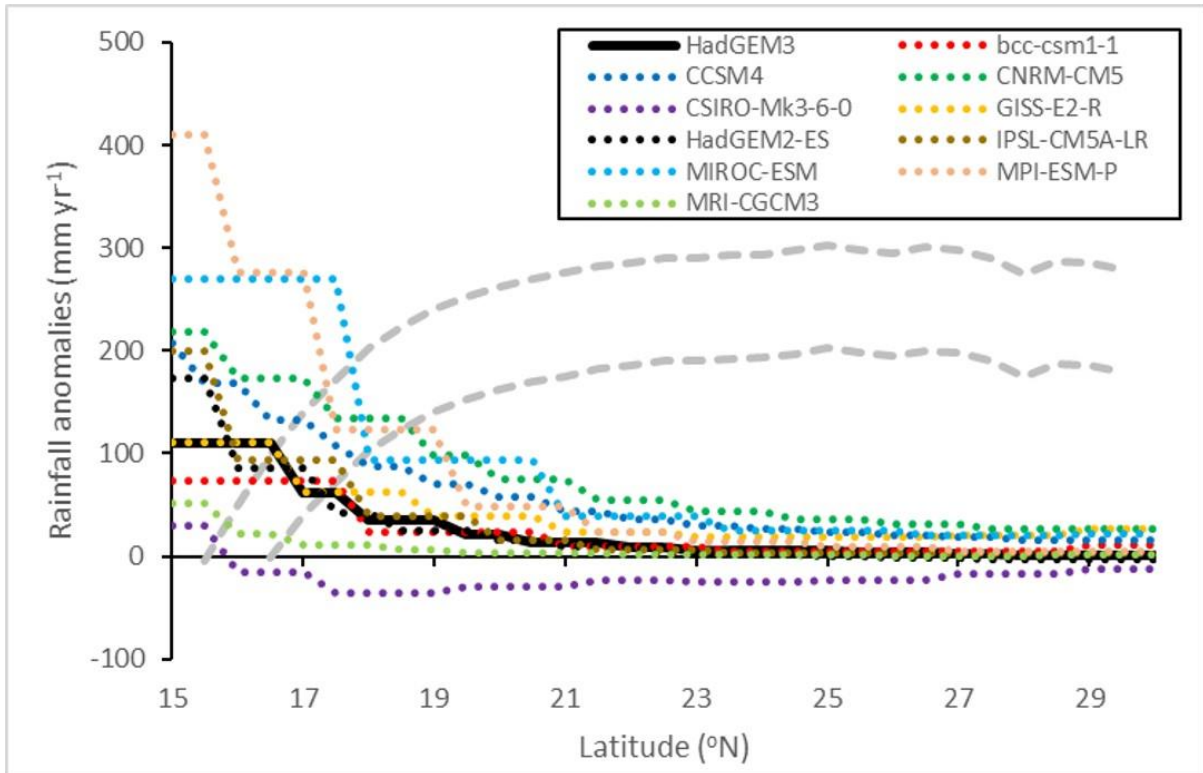
87



88

89 SM6 - Annual mean sea-ice climatology differences, HadGEM3 *midHolocene* production run versus
 90 HadGEM3 *piControl* production run. Stippling shows statistical significance (as calculated by a
 91 Student's T-test) at the 99% level

92



93

94 SM7 - Annual mean rainfall over West Africa (averaged over 20°W-30°E, consistent with Jousaume
 95 *et al.* [1999]), HadGEM3 *midHolocene* simulation minus corresponding *piControl*, and likewise for
 96 previous models from CMIP5. Solid line shows HadGEM3, dotted lines show CMIP5 simulations.
 97 Grey dashes show maximum and minimum bounds of the increase in rainfall required to support
 98 grassland at each latitude, within which simulations must lie if producing enough rainfall to support
 99 grassland (adapted from Figure 3a in Jousaume *et al.* [1999])

100

101

102

103